Interactions between PEI and biological polyanions and the ability of glycosaminoglycans in destabilizing PEI/peGFP-C3 polyplexes for genetic material release

Paulina Alejandra Montaño González, Lizeth Montserrat Bravo-Lozano, Soizic Chevance, Francois Dole, Julien Rosselgong, Pascal Loyer, Sylvain Tranchimand, Jean-Paul Chapel, Fabienne Gauffre, Christophe Schatz, et al.

Author version of article published in *International Journal of Biological Macromolecules* 301 (2025) 140351

Interactions between PEI and biological polyanions and the ability of glycosaminoglycans in destabilizing PEI/peGFP-C3 polyplexes for genetic material release

Paulina Alejandra Montaño-González[a], Lizeth Montserrat Bravo-Lozano[b], Soizic Chevance[a], François Dole[c], Julien Rosselgong[a], Pascal Loyer[d], Sylvain Tranchimand[e], Jean-Paul Chapel[c], Fabienne Gauffre[a], Christophe Schatz[f], Lourdes Mónica Bravo-Anaya[a]*

[a] Univ Rennes, CNRS, ISCR (Institut des Sciences Chimiques de Rennes), UMR 6226, F-35000 Rennes, France

[b] Universidad de Guadalajara, CUCEI, Marcelino García Barragán 1421, CP 44430, Guadalajara, Jalisco, México

[c] Centre de Recherche Paul Pascal (CRPP), UMR CNRS 5031, Université de Bordeaux, 33600 Pessac, France

[d] Univ Rennes, Inserm, INRAE, Institut NUMECAN, UMR-A 1341, UMR-S 1317, Plateforme SynNanoVect, F-35000 Rennes, France

[e] Univ Rennes, École Nationale Supérieure de Chimie de Rennes, CNRS, ISCR, UMR 6226, F-35000 Rennes, France

[f] Univ Bordeaux, Bordeaux INP, LCPO, CNRS, UMR 5629, F-33000 Pessac, France

Corresponding author:

* Dr. Lourdes Mónica Bravo-Anaya, Email : lourdes-monica.anaya@univ-rennes.fr , Tel: +33-656-886-206.

Abstract

The lack of understanding of polyplexes stability and their dissociation mechanisms, allowing the release of DNA, is currently a major limitation in non-viral gene delivery. One proposed mechanism for DNA-based polyplexes dissociation is based on the electrostatic interactions between polycations and biological polyanions, such as glycosaminoglycans (GAGs). This work aimed at investigating whether GAGs such as heparin, chondroitin sulphate and hyaluronic acid promote the dissociation of PEI/DNA polyplexes. We studied the electrostatic complexation between branched poly(ethyleneimine) (*b*-PEI$_{25}$) and polyanions (model DNA and GAGs) through conductivity and ζ-potential measurements. The formation of *b*-PEI$_{25}$/polyanion polyplexes through electrostatic interactions was analyzed in depth, providing key insights into charge stoichiometry, morphology, thermodynamics and physicochemical characteristics. The stability of polyplexes was tested in the presence of the different GAGs. Heparin was found to

be the only polyanion capable of releasing peGFP-C3 plasmid from polyplexes, complexing stoichiometrically with the free *b*-PEI_{25} in excess, before releasing the plasmid. The ability of GAGs to disrupt polyplexes and release DNA was correlated with the thermodynamic characteristics of *b*-PEI_{25}/polyanions complexation. Our findings indicate that heparin's strong interaction with PEI and its high charge density, compared to other GAGs and polyanions, are pivotal in determining complex stability and promoting DNA release.

Keywords: Plasmid peGFP-C3, Biological Polyanions, Electrostatic Interactions, Polyplexes, Gene delivery,

1. Introduction

Gene delivery systems based on synthetic vectors, where nucleic acids are densely packed into polyplexes, lipoplexes or lipid nanoparticles (LNPs) have been increasingly evaluated for nucleic acid-based therapies [1-3]. All these therapies share the same need of having a safe (*i.e.* nontoxic) and efficient delivery of nucleic acids to the cytoplasm or the nucleus of the targeted cells [4]. Although a great deal of progress has been made in this field, the efficiency of these synthetic systems remains much lower than that achieved by viral systems. For polycation-mediated transfection, only 1% of loaded plasmids reach the nucleus and just 0.01 % penetrate it successfully and fulfil their biological function within the cell [5].

Conventional approaches for the transfection of nucleic acids using polyplexes rely on their direct complexation with polycations like poly(ethyleneimine) (PEI), chitosan or poly(L-lysine) (PLL) [6-9]. Polyplexes are mainly internalized by endocytosis, which is an effective means of accessing the intracellular environment [5,10,11]. Once internalized, polyplexes are trapped in endosomes, which are subsequently fused with lysosomes, where lysosomal enzymes degrade polyplexes cargo [12-14]. Consequently, polyplexes must efficiently escape from endosomes to avoid degradation and release nucleic acids allowing them to access the cytosol and the cell nucleus (for plasmid DNA) [13]. Various mechanisms have been proposed and investigated to explain the escape of polyplexes from endosomes. One of the most prominent is the "proton sponge" effect, which suggests that polycations act as a "buffer" by absorbing free protons within the endosomes, leading to an osmotic swelling and eventual rupture of the endosomal membrane, facilitating the release of complexes into the cytoplasm [15-17]. Another possible mechanism

involves the direct interaction of polyplexes with the endosomal membrane, which can lead to destabilization and leakage [15].

While the literature on polyplexes formation is well documented [15-17], few studies have focused on the physical chemistry underlying complex disassembly, particularly under the physicochemical conditions found in the intracellular environment. The dissociation of DNA from polyplexes has been attributed in part to the presence of anionic biomolecules present in the cytoplasm that can compete with DNA to bind to the polycation. This competition weakens the polyplex structure, resulting in the release of DNA [1,18]. Among them, glycosaminoglycans (GAGs) present both in the extra- and intracellular matrix are considered to be competitive biological polyanions that could significantly influence the stability and behavior of complexes in a biological environment [19]. GAGs can compete with nucleic acids if the polycation-GAG association is thermodynamically favored [20]. The GAGs of biological relevance are mainly hyaluronic acid (HA), heparin (HP) and chondroitin sulfate (CS) which are linear polymers composed of repeating disaccharides, with negative charges due to the presence of carboxyl and sulfate groups [19,21] (Fig. 1). However, most studies on the stability of polycation/DNA polyplexes in the presence of GAGs remain descriptive and provide little or no quantitative information on DNA release, or on the binding affinity of polycations to DNA and to competing polyanions.

To date, only Ma *et al.* have explored the capacity of certain biological polyanions, specifically HA, HP and CS, to disrupt chitosan/DNA polyplexes, demonstrating that their effectiveness is closely linked to their binding affinity for chitosan [20]. Their studies assessed the stability of chitosan/DNA polyplexes by measuring the amount of released DNA when exposed to GAGs, through fluorescence spectrophotometry using PicoGreen® (which associates to DNA as an intercalator), when exposed to GAGs. They reported that only the highly charged HP could effectively release DNA from polyplexes. Additionally, HP displaced DNA from polyplexes in a manner dependent on its concentration and the N/P charge ratio, as they note them, where N represents to the concentration of positively charged amino groups from chitosan and P corresponds to the concentration of negatively charged phosphate groups from DNA [22,23]. Higher N/P ratios improve complex stability by allowing free chitosan to bind HP without disrupting the complexes; only after complexing free chitosan additional HP competitively

release DNA [20]. Their findings indicate that free chitosan may help preventing premature dissociation of polyplexes when interacting with anionic biomacromolecules in physiological environments.

Poly(ethyleneimine) (PEI) is one of the most extensively studied synthetic polymeric carriers for gene delivery despite its known *in vivo* toxicity [25,26]. From a fundamental perspective, PEI is particularly significant as it can be synthesized in various structural forms - both linear and branched (*l*-PEI and *b*-PEI, respectively) - while offering a wide range of molecular weights [27] (Fig. 2). This diversity makes it particularly interesting for establishing fundamental correlations between structure and transfection efficiency. PEI is classified as a weak polyelectrolyte, meaning that its protonation rate is highly dependent on the pH and ionic strength of the solutions [28,29]. This polycation has been shown to effectively condense DNA, forming stable PEI/DNA polyplexes. Several research groups have investigated how the molecular weight of PEI affects the physicochemical and biological characteristics of these complexes [30-32]. However, the interactions of PEI with competitive biological polyanions remain poorly documented [33]. Bertschinger *et al.* showed that factors such as pH, osmolarity, and the presence of HP could induce partial disassembly of PEI/DNA polyplexes [34].

In this work we investigate the dissociation of PEI/plasmid peGFP-C3 polyplexes in presence of three GAGs: HA, HP and CS. Branched PEI with a molecular weight of 25 kg/mol (*b*-PEI_{25}) was chosen as the model PEI since it is considered the 'gold standard' in gene delivery systems, providing the highest transfection efficiency [35-38]. Its high charge density and branched structure enable PEI to efficiently condense DNA into small polyplexes [39]. Calf-thymus DNA (CT-DNA ~ 10 kbp), selected as a model DNA chain [40], and plasmid DNA encoding for green fluorescent protein (pEGFP-C3, 4 727 bp) were chosen as the nucleic acids. To understand the dissociation mechanism of polyplexes in presence of GAGs, we need to understand the interaction of PEI with nucleic acids and GAGs. This aspect will be studied in a first part, where the electrostatic complexation of *b*-PEI_{25} with polyanions will be investigated at different charge ratios through conductivity, ζ-potential and dynamic light scattering (DLS) measurements. Then, the dissociation of *b*-PEI_{25}/DNA and *l*-PEI_{20}/DNA polyplexes in the presence of GAGs will be analyzed using gel electrophoresis. The ability of certain GAGs to release plasmid from PEI/DNA polyplexes will be correlated with thermodynamic information determined using

isothermal titration calorimetry (ITC). These findings will be essential for understanding the conditions under which polyplexes dissociate, and hence for designing new strategies for polymeric vectors to achieve efficient gene delivery.

2. Materials and methods

2.1. Materials

Most of the polymers were purchased from Sigma Aldrich including deoxyribonucleic acid sodium salt from calf thymus (CT-DNA), with an average molecular weight (Mw) of 6.6 x 10^3 kg/mol (Sigma-Aldrich, D1501) [22,23,40], branched PEI with a Mw of 25 kg/mol (*b*-PEI_{25}) (Sigma-Aldrich, 408727), linear PEI-hydrochloride with a Mw of 20 kg/mol (*l*-PEI_{20}) (Sigma-Aldrich, 764965), chondroitin 4-sulfate (CS) sodium salt form shark cartilage (Sigma-Aldrich, C4384), hyaluronic acid (HA) sodium salt from rooster comb (Sigma-Aldrich, H5388), porcine heparin (HP-por) (Sigma-Aldrich, H3393), NaOH in pellets with impurities ≤0.001%, anhydrous NaCl (99%) and HCl (37%). Heparin sodium salt (HP) was purchased from MedChem Express (HY 17567A/CS-3922). GAGs Mw were determined by size exclusion chromatography measurements and reported later in this paper. The eGFP-C3 plasmid (4727 bp), having an average Mw of 3.1 x 10^3 kg/mol [41], was purified from an *E. coli* culture with the "Giga AX 10000" NucleoBond®AX. The purified plasmid eGFP-C3 was dissolved in deionized sterile water, and its purity and concentration were determined by UV spectrophotometry using the Nanodrop instrument (Mettler Toledo). Deionized (DI) water (18 MΩ-cm) was used to prepare all the solutions and was obtained by passing in-house deionized water through ELGA PURELAB Option Q7 purification unit.

2.2. Solubilization of PEI and polyanions

Solutions of *b*-PEI_{25} and *l*-PEI_{20} were prepared at a concentration of 1 mg/mL in deionized (DI) water and then adjusted to a pH of 7.4. CT-DNA solutions were prepared at a concentration of 1 mg/mL in DI water with or without addition of 10 mM NaCl. The purified eGFP-C3 plasmid was solubilized in water at a concentration of 0.0345 mg/mL. Solutions of GAGs were prepared at 1 mg/mL in DI water. All the vials containing the solutions were sealed with Parafilm® to prevent solvent evaporation and stored at 4 ºC.

2.3. Size exclusion chromatography (SEC)

SEC analyses of HP, CS and HA were performed at 25°C using a high-performance liquid chromatography system with Shodex SB 806 M HQ and SB 805 HQ columns and Shodex SB-G 6B as precolumn. The mobile phase was composed of $NaNO_3$ 0.1M with NaN_3 100 ppm eluted with a flow rate of 0.8 mL/min. GAGs samples were solubilized in the mobile phase and injected at a concentration of 1 mg/mL. The system includes a multi-angle light scattering detector (Wyatt Heleos 2) and a differential refractive index detector (Shimadzu, RID20A). A refractive index increment (*dn/dc*) of 0.14 mL/g was used for determining the molecular weight of GAGs by light scattering.

2.4. Potentiometric titrations of b-PEI$_{25}$ and l-PEI$_{20}$

b-PEI$_{25}$ and *l*-PEI$_{20}$ (hydrochloride form) were potentiometrically titrated either with 0.1 M HCl and 0.1 M NaOH, respectively using portable pH-meter instrument (HANNA, HI8424N). *b*-PEI$_{25}$ and *l*-PEI$_{20}$ solutions were prepared in water at a concentration of 1 g/L. The protonation rate of *b*-PEI$_{25}$ and *l*-PEI$_{20}$ was determined as a function of pH [42]. The concentration of protonated amine groups, $[NH^+]$, including primary, secondary and tertiary amines was calculated by applying electroneutrality, $[NH^+] = [OH^-] + [Cl^-] - [H^+]$. Then, the protonation rate (σ) was defined by $\sigma = [NH^+]/[N]^0$ where $[N]^0$ corresponds to the total amine concentration, determined from the molar concentration of repetitive units in *b*-PEI$_{25}$ and *l*-PEI$_{20}$.

2.5. Conductimetry

Conductimetric measurements were performed to determine the complexation stoichiometry of *b*-PEI$_{25}$/polyanions polyplexes, using a SevenGo Duo pH/Cond meter SG23-EL-Kit from Mettler Toledo. The *b*-PEI$_{25}$ solution prepared at 0.94 mg/mL and adjusted at pH 7.4 was added stepwise in the polyanion solution (0.03 mg/mL for CT-DNA and CS, 0.01 mg/mL for HA and HP) under continuous stirring. The added volumes of *b*-PEI$_{25}$ were converted into molar charge ratios, R = [+]/[-] where [+] represents the molar concentration of protonated amine groups, and [-] corresponds to the molar concentration of anionic groups from DNA or GAGs. For the GAGs, it was assumed that sulfuric and carboxylic groups were fully ionized at pH 7.4.

2.6. Zeta potential

A Zetasizer NanoZS instrument (Malvern) was used to measure the ζ-potential of polyplexes by laser doppler electrophoresis using the PALS (Phase analysis light scattering) technology. The *b*-PEI_{25} solution (0.94 mg/mL, pH 7.4) was incrementally added to the polyanion solution (V= 5 mL, 0.01 or 0.03 mg/mL, consistently with the conditions used for conductivity measurements) under continuous stirring to reach different R values. After each addition, the suspension of polyplexes was stirred for 5 minutes to ensure stabilization. The electrophoretic mobility was measured and converted to ζ-potential values using the Smoluchowski equation [43]. Each measurement was repeated three times, and the sample was subsequently returned to the initial suspension. ζ-potential results are reported as mean values ± standard deviation from two independent formulation replicates.

2.7. Polyplexes preparation through ¨one-shot and vortex¨ mixing route

The *b*-PEI_{25}/polyanions polyplexes were prepared at different charge ratios (R = 0.5, 0.8, 3, 5 and 10) as follows. The appropriate volume of *b*-PEI_{25} solution was rapidly added using a micropipette to 1 mL of the polyanion solution, and the suspension was vortexed for 30 s. The *b*-PEI_{25}/peGFP-C3 polyplexes were prepared using the same methodology at charge ratios of 3, 5, 10 and 15 for DLS and ζ-potential measurements, and at charge ratios of 3, 4, 5, 8, 9, 10, 14, 15, 18 and 20 for gel electrophoresis stability assays.

2.8. Dynamic light scattering (DLS)

DLS measurements were conducted at 25 ºC using the same ZetaSizer Nano ZS instrument as that used for the zeta potential measurements. The instrument is equipped with a HeNe laser (λ_0 = 632.8 nm) with a detection angle of 173° (non-invasive backscatter technology). The correlation functions were averaged from two measurements, each one consisting of 2 runs (30 seconds per run), following a 2-minute equilibration period at 25 °C. NNLS (non-negative least squares) and cumulants algorithms were applied to extract the intensity-weighted particle size distribution (PSD) and the intensity-weighted mean hydrodynamic size (Z-average diameter), respectively. The hydrodynamic diameter is obtained from the Stokes−Einstein equation assuming spherical particles [43,44]: $D_H = \frac{k_B T}{3\pi\eta_s D}$ where k_B is the Boltzmann constant, T is the temperature, η s is the viscosity of the solvent and D is the apparent diffusion coefficient. The values of hydrodynamic diameter (D_H) and polydispersity index (PDI, obtained by the cumulants

analysis) are presented as mean values with ± standard deviation from two independent formulation replicates.

2.9. Atomic Force Microscopy (AFM) measurements

Polyplexes were prepared at a charge ratio of 4 and were deposited on mica surfaces and imaged in air at room temperature using a Dimension ICON AFM (Bruker, Billerica, USA). Imaging was made in PeakForce mode to precisely control the force acting on the chains (setpoint) using SCANASYST-AIR probes having a tip radius of ~1–2 nm (Bruker, Billerica, MA, USA) at a scanning rate of 0.4 Hz. Mica substrates were freshly cleaved prior to all experiment to expose a genuine, and molecular smooth surface. Polyplexes were prepared by solvent casting from a dilute stock solution (0.03 mg/mL) to minimize aggregates and isolate particles on the mica surface for better imaging. A volume of 4 µL of suspension was deposited on freshly cleaved mica and allowed to dry under nitrogen flow for several minutes. The polyplexes were positively charged in solution, ensuring a strong electrostatic interaction with the negatively charged mica surface. Apparent diameters and heights were estimated using the particle cross-section analysis tool supplied with Nanoscope Analysis software (Version 1.90, Bruker).

2.10. Transmission Electron Microscopy (TEM) measurements

TEM images were captured using a JEOL 1400 TEM operating at 120 kV and equipped with a GATAN Orius 1000 camera. 7 µL of *b*-PEI_{25}/eGFP-C3 polyplexes prepared at a R of 10 were directly deposited onto copper grids with carbon coating (300 mesh Cu-300LD from Pacific Grid Tech), allowed to dry at room temperature and then blotted after 15 min. The particle size distribution was analyzed by measuring individual particles using Image-J software on the TEM micrographs.

2.11. Nanoparticle Tracking Analysis (NTA) measurements

NTA measurements were performed with a Nanosight LM10 device system (Malvern Panalytical) equipped with a 40 mW laser working at λ= 638 nm. A CCD camera operating at 30 frames per second was used to record video sequences of the light scattered by polyplexes, appearing as individual spots. Video sequences were then evaluated via the NANOSIGHT NTA 2.0 Analytical Software Suite. Measurements were performed at 25 °C. The size of each polyplex

was individually deduced from the analysis of its Brownian motion [45]. *b*-PEI_{25}/polyanions polyplexes analyzed with this method were formulated at R=5, by rapidly mixing a specific volume of a *b*-PEI_{25} solution with 1 mL of the polyanion solution, followed by vortexing the suspension during 30 s. Samples were prepared at a dilution factor of 400 prior to NTA measurements. NTA yields size distribution in numbers.

2.12. Agarose gel electrophoresis

b-PEI_{25}/peGFP-C3 and *b*-PEI_{20}/peGFP-C3 polyplexes stoichiometry assays were performed using gel retardation assays. Briefly, increasing amounts of either *b*-PEI_{25} or *l*-PEI_{20} at a concentration of 0.024 mg/mL were added to 100 ng of peGFP-C3 plasmid DNA (20 μL) to prepare polyplexes at various charge ratios R. Polyplexes were then incubated for 10 min at room temperature. Then, 4 μL of 4X-loading buffer (0.1 mM EDTA, 0.05 % bromophenol blue, 50 % glycerol) were added to the mixture. 10 μL of the suspension were applied to a 0.8 % agarose gel in 1x TAE buffer (40 mM Tris, 20 mM acetic acid, 1 mM EDTA). SYBR® Safe (Life Technologies, CA, USA) was used to reveal the DNA bands. The gel electrophoresis was run at 100 V for 45 min. Gels were analyzed using the Molecular Imager® Gel Doc™ XR+ and the Image Lab™ Software.

Stability assays to induce plasmid release from *b*-PEI_{25}/peGFP-C3 polyplexes in presence of GAGs were also carried on with gel electrophoresis. *b*-PEI_{25}/peGFP-C3 polyplexes were prepared as described above, then, increasing volumes of GAGs were added to the sample to destabilize polyplexes. GAGs were used at the following concentrations: 0.8 mg/mL for HA, 1.3 mg/mL for CS, 0.1 mg/mL for HP and HP-por. *b*-PEI_{25}/peGFP-C3 polyplexes with GAGs were incubated for an additional 10 min at room temperature. Finally, 4.5 μL of loading buffer were added to the mixture and an aliquot of 10 μL were applied to the 0.8 % agarose gel electrophoresis in 1x TAE buffer. In the gels, the concentration of GAGs present in the polyplexes is expressed in molar concentration in charges.

2.13. Isothermal Titration Calorimetry (ITC) measurements

b-PEI_{25}/polyanions binding studies were conducted at 25 °C using a Nano ITC microcalorimeter from TA instrument. All solutions were prepared in 100 mM HEPES buffer at pH 7.4 using the following concentrations (mass concentration, molar concentration in repetitive units): *b*-PEI_{25}

(1.12 mg/mL, 26 mM), HP (0.322 mg/mL, 1.90 mM), CS (0.426 mg/mL, 1.84 mM), HA (0.385 mg/mL, 0.96 mM), CT-DNA (0.587 mg/mL, 1.78 mM). The concentrations were optimized to obtain sigmoidal shape isotherms with a high signal-to-noise ratio. All solutions were degassed using a dedicated degassing station from TA instrument, prior to measurements. Each titration consisted of an initial injection of 1.1 μL of *b*-PEI_{25} in the polyanion solution, followed by 19 injections of 10 μL at intervals of 300 s. In order to obtain net binding heats, the heats of dilution from titration of *b*-PEI_{25} into the HEPES buffer and HEPES buffer into polyanions were subtracted from the binding isotherm. The data were analyzed with Origin software using a modified [45, 46] multiple non-interacting sites (MNIS) model [47, 48], which allowed for a more comprehensive consideration of distinct contributions: the electrostatic complexation step (ion-pairing) and the condensation/reorganization steps. This model was preferred over the more classical two-side binding model because the two processes did not occur simultaneously throughout the titration but sequentially.

3. Results and discussion

3.1. Electrostatic complexation of b-PEI_{25} with DNA and GAGs

3.1.1 Polyelectrolytes characteristics

The average molar masses in terms of weight (Mw) and number (Mn), as well as the dispersity index (Đ), of the GAGs were determined using SEC-MALS analysis (Table 1 and Fig. S.I. 1). HA was found to be notably of much higher molar mass than other GAGs. The two heparin samples, HP and HP-Por differ by an order of magnitude in terms of molar mass, which is interesting for understanding how the molecular weight of GAGs affects the dissociation of polyplexes. The disaccharide units of GAGs contain carboxylic and sulfuric acid groups which are completely ionized in aqueous solution at pH 7.4, since the pK_a values for carboxylic groups are between 2.79 to 3.13 [20, 49, 50], while those of sulfuric groups are between 0.5 and 1.5 [51]. Among the GAGs, HP displays the highest negative charge density due to the presence of multiple sulfate groups in addition to a carboxylate group in each disaccharide unit [52]. The charge density of HP translates into a Manning parameter of $\Gamma_M = 3.2$, which significantly exceeds the threshold for counterion condensation ($\Gamma_M = 1$) [21]. CS contains fewer sulfate groups per disaccharide unit ($\Gamma_M = 1.5$). In contrast to HP and CS, HA has the lowest negative

charge density (Γ_M = 0.7), featuring only one carboxylate group on the glucuronic acid residue within each repeating disaccharide unit [53]. DNA has the highest charge density due to its duplex structure (Γ_M = 4.1).

b-PEI$_{25}$ is a weak polybase with a complex ionization behavior attributed to its branched structure, with the presence of primary, secondary and tertiary amines in a ratio of 1:2:1 [54,55]. A notable feature of PEI polymers is that, under acidic conditions, only about two-thirds of the available amines can be ionized [42,56]. This was very well verified experimentally by titrating *b*-PEI$_{25}$ with 0.1 M HCl using conductimetry and potentiometry, performed in separate experiments. In both cases, the titration endpoint was reached for 0.72 equivalent HCl relative to the molar amount of amine groups (Fig. S.I. 2). By applying the electroneutrality conditions to the data resulting from potentiometric titrations, the degree of protonation at the titration endpoint was found to be 0.70 (Fig. S.I. 2). The incomplete protonation of amines in *b*-PEI$_{25}$ can be attributed to two main factors. Firstly, the proton affinity of the polymer decreases with increasing protonation, mainly due to the electrostatic interactions between neighboring protonated sites, which limits further protonation, as observed for any polyamines [57]. Secondly, amine accessibility plays a crucial role; primary and secondary amines located on the surface are more readily accessible for protonation, while tertiary amines, which are buried within the *b*-PEI$_{25}$ structure, are less accessible, further contributing to the incomplete protonation. More precisely, it has been shown that primary amines in *b*-PEI$_{25}$ protonate at high pH, while secondary amines start protonating at around pH 8-10. Tertiary amines only protonate at very low pH due to their proximity to protonated sites, making them highly acidic. At pH 7.4, where the degree of protonation of *b*-PEI$_{25}$ is only 0.30 (Fig. S.I. 2), *b*-PEI$_{25}$ behaves as weakly charged polyelectrolyte, with a Manning parameter below the counterion condensation threshold (Γ_M = 0.8) [20].

3.1.2 Complexation stoichiometry

When two oppositely charged polyelectrolytes interact, several phenomena contribute to the complexation process. Firstly, electrostatic interactions or ion- pairing form between the oppositely charged units, significantly reducing the (enthalpic) Coulomb energy of the polyelectrolyte chains [59]. Subsequently, the counterions initially associated/condensed with the charged groups are released as the same time as the dehydration of the charged groups,

resulting in the release of water molecules. This release of counterions and water molecules leads to a significant increase in the translational entropy of the system, playing a major role in the complexation process compared to the enthalpic counterpart. The formation of polyelectrolyte complexes (PECs) is therefore most of the time driven by entropy [60-63]. One of the key parameters to consider when characterizing PECs formation is the complexation stoichiometry, defined as the molar ratio of oppositely charged group that interact effectively to form the complex. The electrostatic interactions within PECs can be interpreted in two distinct ways: as either a continuous field of charges or as discrete charge or ion pairing, often referred to as salt bonds [64]. In practice, the field interpretation is more applicable to weak polyelectrolyte complexes, which tend to form liquid coacervate droplets through a liquid-liquid phase separation (LLPS), while the ion-pairing model better describes strong PECs that result in solid precipitate at charge stoichiometry. Regardless of the interpretation, the complexation stoichiometry can be determined using straightforward analytical techniques, such as conductimetry, turbidity measurements, and electrophoresis [22,23,65-67].

Here, conductimetry and electrophoretic mobility measurements were used independently to determine the stoichiometry for polyplexes formed from *b*-PEI$_{25}$ and various polyanions (CT-DNA, HA, CS and HP). In both cases, the polyanion was titrated by *b*-PEI$_{25}$ at pH 7.4. In general, titration data are plotted as function of the charge ratio R ([+]/[-]), defined as the ratio of the concentration of positive charges brought by PEI to the concentration of negative charges brought by polyanions. For *b*-PEI$_{25}$/CT-DNA polyplexes, the charge ratio is denoted as $[N^+]/[P^-]$, where $[P^-]$ corresponds to the concentration of negatively charged phosphate groups. For the *b*-PEI$_{25}$ /HA polyplexes, since HA contains only carboxyl groups in its chain, the charge ratio is denoted as $[N^+]/[C^-]$, where $[C^-]$ corresponds to the concentration of negatively charged carboxylic groups. For *b*-PEI$_{25}$ /CS and *b*-PEI$_{25}$ /HP polyplexes, as both GAGs contain sulfate groups and a carboxyl group per each monomeric unit, the charge ratio is denoted as $[N^+]/([C^-]+[S^-])$, where $[S^-]$ corresponds to the concentration of negatively charged sulfate groups.

Fig. 3a to 3d show the variations in electrical conductivity as a function of charge ratio during *b*-PEI$_{25}$/polyanion polyplexes formation. For each titration, a solution of *b*-PEI$_{25}$ adjusted to pH 7.4, which corresponds to a protonation level of 30%, was gradually added to a polyanion solution prepared in water. CT-DNA was selected as a well-known and commercially available

model of linear nucleic acid [40], to study the nature of interactions and charge stoichiometry with *b*-PEI$_{25}$. The initial increase in conductivity reflects the complexation process with the release of counterions, specifically Na^+ from polyanions and Cl^- from *b*-PEI$_{25}$ [22,65-67]. In the second part of the titration, the lower increase in conductivity is attributed to the addition of the excess PEI, as observed by Bravo-Anaya *et al.* during chitosan/DNA polyplexes formation [22]. The intersection point of the two trends defines the equivalence of the system, at which all titratable charges of the polyanions are fully complexed by the opposite charges of the PEI. This intersection point allows for the determination of the complexation stoichiometry. If the equivalence is reached precisely at R = 1, it indicates that the polyplex composition is perfectly stoichiometric, with each negative charge balanced by a corresponding positive charge. For CT-DNA (Fig. 3a) and HA (Fig. 3d), where the phosphate and carboxylate contents are well-defined, the equivalence point is achieved at R = 1, indicating stoichiometric complexation. This outcome demonstrates that the complexation process is entirely driven by electrostatic interactions. In contrast, for HP and CS, the initial sulfate content was not precisely known and was estimated based on their chemical structures. Given that the complexation of *b*-PEI$_{25}$ with DNA and HA was stoichiometric, we assumed a similar behavior for HP and CS. This assumption enabled us to calculate the actual sulfate and carboxylate content in these polyanions (2 and 3.5 negative charges per disaccharide, for CS and HP, respectively). The observation that complexation stoichiometry is close to unity for polyplexes despite variations in charge density between polyelectrolytes is a general observation in many systems. This results from the interplay between polymer conformation, dynamic rearrangement, and the influence of the local ionic concentration [68]. Together, these factors facilitate the readjustments necessary to ensure efficient charge pairing, leading to the formation of stable PECs with nearly balanced stoichiometry.

Complexation between *b*-PEI$_{25}$ and the different biological polyanions was also studied with electrophoretic mobility measurements giving access to ζ-potential of the polyplex particles (Fig. 4a to 4d). A titration approach was employed, similar to the procedure previously used for conductivity measurements. For all variations of the ζ-potential as a function of R, we can observe a first plateau with negative ζ-potential values between -40 and -20 mV, depending on the polyanion and its concentration. This plateau is attributed to the formation of partially complexed *b*-PEI$_{25}$/polyanion polyplexes particles, as already observed and reported in the

literature for other systems like chitosan/DNA and cationic ELPs/DNA polyplexes, among others [22,23,69]. The ζ-potential increases after a charge ratio of 0.75. The R values at the crossover point, where the ζ-potential is 0 mV (isoelectric point indicating zero electrophoretic mobility for particles), corresponds to the electrical equivalence at which the negative charges of the polyanions are fully complexed by the PEI. These values are is in good agreement with the data obtained from conductimetric measurements. The positive plateau obtained for [+]/[-] > 1 indicates the overcharging of polyplexes with an excess of PEI. It is worth mentioning that at the isoelectric point, polyplexes tend to aggregate while ongoing with the titration procedure. Such aggregates were excluded from the analysis due to their tendency to sediment.

Since GAGs are abundantly found in the extracellular matrix, in the cytoplasm and on the plasma membrane [70], nucleic acid-based polyplexes can undergo polyion exchange or substitution reactions in the cytoplasm [71]. As mentioned previously, GAGs can compete with nucleic acids, forming polycation/GAGs polyplexes, which can lead to partial or complete dissociation of original polyplexes, if the polycation/GAG association is thermodynamically favored [19,20]. The formation and characterisation of *b*-PEI$_{25}$/polyanion polyplexes, as well as their thermodynamic properties are described in the following sections.

3.1.3 Characterization of b-PEI$_{25}$/polyanion polyplexes

The determination of *b*-PEI$_{25}$/polyanion polyplexes stoichiometry using charge equivalence calculations for CT-DNA and HA, as well as conductimetric and ζ-potential measurements for CS and HP, enabled us to establish the preparation conditions for preparing *b*-PEI$_{25}$/polyanion polyplexes at different charge ratios (R = 0.3, 0.8, 3, 5, and 10). Polyplexes were prepared in the absence of external salts by rapidly adding the *b*-PEI$_{25}$ solution using a micropipette to the polyanion solution, followed by vortex mixing during 30 s.

Fig. 5 shows the intensity-weighted size distribution obtained by DLS of the different polyplexes. The sizes, PDI and ζ-potential values of the different polyplexes are summarized in Table 2. Regardless of the polyanion considered, polyplexes formed at R > 1 have sizes well below 100 nm, with a relatively narrow size distribution (PDI < 0.3). The presumed morphology of these polyplexes is that of a colloidal particle, with a core composed mainly of the polyanion complexed by the *b*-PEI$_{25}$, while the corona is made up of an excess of partially complexed *b*-

PEI_{25}, with free protonated amines giving the polyplexes a positive charge. For values of R greater than 3, the polyplex particles become increasingly compact and sizes decrease with the increase on the charge ratio (Table 2), as observed for other systems such as chitosan/DNA or ELPs/DNA polyplexes [7,22,23]. This demonstrates that a substantial excess of *b*-PEI_{25} is required to effectively complex the polyanion into small, dense particles. This observation suggests that the presence of excess charges from *b*-PEI_{25} on the surface of the polyplex does not necessarily imply complete complexation of the polyanion chains, nor that the polyplexes have reached their most stable or thermodynamically optimal configuration. For values of $R < 1$, it is interesting to note that the polyplexes formed at R = 0.8 with DNA and HA exhibit particularly large hydrodynamic sizes compared with those obtained at R = 0.5. This behavior cannot be attributed solely to the proximity of charge stoichiometry (R = 1), where the system becomes critically unstable, as this was not observed with HP and CS under similar conditions. Rather, it reflects the substantial size and rigidity of the partially complexed DNA and HA chains, suggesting that a higher degree of complexation ($R > 1$) is necessary to condense these polyanions into smaller polyplex particles. Polyplexes characterization was completed using Nanoparticle Tracking Analysis (NTA) giving access to the number-weighted particle size distribution (Fig. S.I. 3). The mean particle sizes of polyplexes prepared at a charge ratio of R=5, were found to be consistent with those obtained by DLS, in relation with the relatively low size dispersity of the system (Table 2). Furthermore, as polyplexes were diluted 400-fold for NTA analysis, it can be concluded that particles are stable under dilution.

3.2.4. Morphology of b-PEI_{25}/polyanion polyplexes

AFM was used to image the solid-state morphology of polyplexes at a charge ratio R=4, which was selected in order to have free *b*-PEI_{25} on the surface of the polyplexes, enabling effective interaction with negatively charged cell membranes (Fig. 6). The analysis revealed the presence of a few particles approximately 100 nm in size, alongside a larger population of smaller particles (< 20 nm) (Fig. S.I. 4). The discrepancy in average polyplex sizes compared to DLS and NTA measurements can be attributed to the adsorption process of polyplexes onto the oppositely charged mica substrate, which likely causes a slight spreading of the particles. This spreading leads to an increase in their lateral dimensions. During the casting of the polyplex droplets onto the mica surface, the evaporation of the solution locally increases the concentration of the salts

it contains (free counterions Na^+ and Cl^- in particular), thereby raising the ionic strength. This process occasionally results in the disassembly of certain electrostatically assembled structures. This observation supports the hypothesis of a complex hierarchical structure, where small primary polyplexes form during the initial stages of complexation and subsequently aggregate into larger secondary polyplex particles, stabilized by an excess of free PEI at the polyplexes surface. This mechanism, first described by Cousin et al. for complexes based on polystyrene sulfonate (PSS) and lysozyme [72], involves a two-step process: an initial fast complexation driven by electrostatic interactions, leading to the formation of small complex particles, followed by their slow aggregation into larger secondary structures (secondary complexes). A similar phenomenon has been observed for polyplexes formed from PSS and poly(diallyldimethylammonium chloride) (PDADMAC) [73, 74], as well as for PSS and PEI by Haddou et al. [75]. The clustering mechanism has never been thoroughly investigated. If the primary polyplexes formed under rapid complexation conditions are neutral, their aggregation may be driven by hydrophobic forces, which act locally to minimize their surface energy. Conversely, if the polyplexes carry a net charge, their aggregation can be mediated by free polyelectrolytes (PE) of opposite charge. In both scenarios, the resulting clusters are stabilized by repulsive electrostatic interactions arising from excess PE when the charge ratio is different from neutrality. AFM analyses of large polyplex particles further corroborated the hierarchical structure, revealing characteristic sizes for the primary and the secondary polyplexes (core and corona) (Fig. S.I. 4, S.I. 5 and Table S.I. 1).

3.3. b-PEI_{25}*/peGFP-C3 polyplexes preparation and characterization*

The peGFP-C3 plasmid was selected as model plasmid DNA since this expression plasmid encoding a red-shifted variant of the wild-type GFP is widely used for transfection experiments in mammalian cells [76]. *b*-PEI_{25}/ peGFP-C3 polyplexes were prepared at four charge ratios ($R=[N^+]/[P^-]$= 3, 5, 10 and 15 with $C_{peGFP\text{-}C3}$ = 0.034 mg/mL) (Fig. 7) to test their stability in presence of the different GAGs. Complete complexation and plasmid DNA charge neutralization with *b*-PEI_{25} occurs at R=1. However, higher charge ratios (R >1) were selected for preparing *b*-PEI_{25}/peGFP-C3 polyplexes to ensure an excess of *b*-PEI_{25}, impairing a positive charge to the polyplexes [10] [77]. Fig. 7a shows the evolution of ζ-potential as a function of charge ratio ($[N^+]/[P^-]$) during the titration of peGFP-C3 with *b*-PEI_{25}. As for previous *b*-PEI_{25}/polyanion

polyplexes, we can observe a first plateau with negative ζ-potential values around -20 mV, corresponding to the formation of partially complexed peGFP-C3 with *b*-PEI$_{25}$ [22,23,65]. ζ-potential values increase after a charge ratio of around 0.75. The isoelectric point is obtained at R=1, consistent with previous result obtained for CT-DNA. The overcharging is also observed at R > 1 with a second ζ-potential plateau around a value of + 20 mV.

Gel retardation assays were also performed at different charge ratios to evaluate *b*-PEI$_{25}$/peGFP-C3 binding properties and identify complexation stoichiometry. SYBR® Safe, a fluorescent DNA stain that binds specifically to the DNA double helix, enables the visualization of plasmid DNA during the gel electrophoresis process. As shown in Fig. 7b, the *b*-PEI$_{25}$ can effectively complex peGFP-C3 at a charge ratio $[N^+]/[P^-]=1$, in good agreement with ζ-potential measurements (Fig. 7a). The presence of fluorescence in the gel lane at R < 1 suggests incomplete DNA complexation, allowing SYBR to bind free or weakly bound plasmid DNA, which is observed migrating through the gel. Additionally, fluorescence is clearly detected in the wells, indicating the presence of complexes that are too large to migrate and sufficiently loose to allow the diffusion of the dye within them (Fig. 7b). In contrast, at R>1, when polyplexes are stable, the strong interaction between PEI and plasmid DNA restricts the diffusion of SYBR within the polyplexes, resulting in no detectable fluorescence in the wells.

Fig. 7c shows size distribution obtained by DLS of *b*-PEI$_{25}$/peGFP-C3 polyplexes at charge ratios of 3, 5, 10 and 15. *b*-PEI$_{25}$/peGFP-C3 polyplexes present hydrodynamic sizes below 100 nm, with a monomodal distribution and PDI values lower than 0.3. The particle size decreases as the charge ratio increases, consistent with previous observations for *b*-PEI$_{25}$/polyanion polyplexes. The reduction in polyplex size primarily results from a more effective of a fixed number of plasmid molecules across an increasing amount of *b*-PEI$_{25}$ when the charge ratio increases. Additionally, the size reduction may also be partially attributed to a higher degree of compaction of the primary polyplexes within the polyplexes, as discussed before [74]. TEM observations carried on polyplexes prepared at a charge ratio of 10 show uneven nanosized polyplexes in a dried state (Fig. 7d). AFM observations revealed the presence of core-corona particles, where the core is composed mainly of peGFP-C3 complexed by the *b*-PEI$_{25}$ (Fig. 7e and Fig. S.I. 6).

Table 3 summarizes the hydrodynamic sizes, PDI and ζ-potential values of *b*-PEI$_{25}$/peGFP-C3 polyplexes prepared at various charge ratios. If we compare the obtained polyplexes sizes to other polycation/plasmid systems, *b*-PEI$_{25}$/peGFP-C3 polyplexes present smaller sizes than those of ELPs/DNA polyplexes (135 nm, R=3) and hybrid ELPs/pDNA polyplexes (from 115 to 180 nm) [65,67]. The sizes of polyplexes are also similar to those of some chitosan/CT-DNA polyplexes (from 80 to 120 nm, R=5, depending on chitosan molecular weight) [23] and smaller than PLL/DNA polyplexes (from 60 to 260 nm, R=7, in the presence of various concentration of NaCl) [78].

3.4. GAGs' ability to dissociate b-PEI$_{25}$/peGFP-C3 polyplexes and release the plasmid

3.4.1. Effect of GAGs type

The interactions between DNA/polycation complexes (polyplexes) and cell membranes play a pivotal role in elucidating the molecular mechanisms governing polycation-facilitated delivery of nucleic acid therapeutics into target cells [76]. As previously mentioned, an excess of *b*-PEI$_{25}$ is required to impart a global positive charge to the polyplexes, which is essential for effective interaction with negatively charged cell membranes and subsequent internalization [77]. *b*-PEI$_{25}$/peGFP-C3 polyplexes were firstly prepared at the charge ratio of 4 and exposed to different concentrations of HP, CS and HA to identify the ability of these GAGs to dissociate polyplexes and partially or fully release the peGFP-C3 plasmid. Gel retardation assays were carried on to assess peGFP-C3 release from polyplexes by analyzing the electrophoretic mobility of the plasmid in the presence of GAGs added at various concentrations to the polyplexes. Fig. 8 shows the gel electrophoresis results, demonstrating that, at the selected concentrations, HP was the only GAG able to disrupt *b*-PEI$_{25}$/peGFP-C3 polyplexes and release the plasmid. The partial release of peGFP-C3 takes place with HP at a molar concentration in charges of 0.0498 mM, and the complete release of peGFP-C3 was obtained with 0.0588 mM HP. It is noteworthy that strong fluorescence was observed in the wells at moderate concentrations of HP (0.0405 mM), indicating that the polyplexes were sufficiently loose to allow SYBR diffusion within them. However, this HP concentration was not high enough to achieve complete DNA release. CS was added into *b*-PEI$_{25}$/peGFP-C3 polyplexes up to a concentration of 0.106 mM and HA up to a concentration of 0.151 mM, but no evidence of plasmid release was observed. The absence of significant fluorescence in the wells also indicates that CS and HA are unable to loosen the

polyplex structure. A second sample of CS with a lower molecular weight (27 000 g/mol) was also tested (results not shown), leading to the same results, that is, no peGFP-C3 release. As mentioned previously, among all the GAGs, HP (with a Γ_M = 3.2) exhibits the highest negative charge density due to the presence the carboxylate groups and multiple sulfate groups in each disaccharide unit, which could explain its capacity to disrupt polyplexes and release the plasmid. Although not all GAGs are able to release the plasmid, they are all able to interact with *b*-PEI$_{25}$. Thus, when *b*-PEI$_{25}$/peGFP-C3 polyplexes prepared at R = 4 are exposed to biological polyanions, the polyanions can interact with the excess PEI, leading to the formation of new polyplexes. In a previous study, Ma *et al.* [20] demonstrated that HP can effectively dissociate DNA from the polyplexes by interacting first with excess free polycation before displacing polycation from DNA/polycation polyplexes. Based on the respective concentrations of plasmid and *b*-PEI$_{25}$ in the polyplexes at R = 4, the concentration of free PEI is estimated to be 0.012 mM in charged units at pH 7.4, assuming 30% protonation of *b*-PEI$_{25}$ and a complexation stoichiometry of 1:1 between peGFP-C3 and *b*-PEI$_{25}$. Given that the concentration of HP required to release DNA is 0.0588 mM, this indicates that HP most likely complexes with free PEI first before displacing it within the polyplexes. Our results are in good agreement with reports from literature, in which HP is usually used as a disrupting biological polyanion of gene delivery carriers [33,34,79,80].

3.4.2. Effect of charge ratio

The impact of charge ratio (R=[N^+]/[P^-]) on *b*-PEI$_{25}$/peGFP-C3 polyplexes stability and the ability of HP to dissociate them was studied in a set of polyplexes prepared at R from 3 to 20. Fig. 9 shows the gel electrophoresis results for *b*-PEI$_{25}$/peGFP-C3 polyplexes prepared at R= 3, 5, 9 and 14, as an example, showing that at higher charge ratios, polyplexes exhibit enhanced stability in the presence of heparin. In this sense, higher concentrations of HP are required to partially or totally dissociate the polyplexes and release the plasmid. This higher stability is obviously attributed to the complexation of HP with free *b*-PEI$_{25}$, leading to a lower concentration of HP available for competing with DNA. Our results support the hypothesis that free polycations in the suspension can prevent premature dissociation of nucleic acids polyplexes when exposed to other negatively charged biomacromolecules in the extra- or intracellular environment. For all R values, a significant fluorescence was consistently observed in the wells

when the HP concentration was not high enough to release DNA, confirming that the polyplexes loosened before disruption occurred.

Fig. 10 shows the dependence of the concentration in charges per monomeric unit of heparin (mM) to induce partial and total peGFP-C3 release from polyplexes as a function of charge ratio ($[N^+]/[P^-]$). There is a linear increase in the required amount of heparin to release the DNA as the charge ratio increases, which is directly related to the stoichiometric complexation of HP with excess free PEI in the polyplex suspension, as shown by conductimetry (Fig. 3b).

3.4.3. Effect of heparin molecular weight (Mw)

The impact of heparin Mw on *b*-PEI_{25}/peGFP-C3 polyplexes stability was also studied by using two heparin samples, namely HP ($M_w \approx 6\,200$ g/mol) and HP-Por (Mw= ≈ 33 600 g/mol) (Table 1). Fig. 11 shows the gel electrophoresis results for *b*-PEI_{25}/peGFP-C3 polyplexes prepared at R=4, showing that the peGFP-C3 release in presence of HP-Por starts at the same molar concentration than low Mw HP (0.0498 mM). The Mw of HP does not seem to impact the disruption of polyplexes and the release of plasmid. Higher Mw (> 10^5g/mol), as well as lower Mw (<10^3 kg/mol) should be tested to draw more definitive conclusions. It is noteworthy to mention that heparin has a much smaller Mw than peGFP-C3 DNA, yet it can still compete effectively for complexation with PEI. This clearly demonstrates that the charge density of polyelectrolytes is a more significant factor than Mw.

3.4.4. Effect of PEI structure

A linear PEI sample with a molecular weight of 20 kg/mol (*l*-PEI_{20}), close to that of the branched structure used throughout this paper (25 kg/mol), was selected to study the impact of PEI chemical structure on PEI/peGFP-C3 polyplexes stability and plasmid release in presence of HP. Prior performing gel electrophoresis assays of *l*-PEI_{20}/peGFP-C3 polyplexes with HP, polyplexes stoichiometry was determined through ζ-potential measurements, confirming an effective complexation at R=1, in good agreement with gel electrophoresis assays. Furthermore, *l*-PEI_{20}/peGFP-C3 polyplexes were also prepared through the rapid addition of *l*-PEI_{20} to the peGFP-C3 solution using the one shot and vortex method, and characterized by DLS measurements (Fig. S.I. 7). Fig. 12 shows the gel electrophoresis results, for *b*-PEI_{25}/peGFP-C3 and *l*-PEI_{20}/peGFP-C3 polyplexes prepared at R= 4, in presence of increasing amounts of HP.

While for polyplexes prepared with *b*-PEI$_{25}$, 0.0543 mM of HP is needed to start releasing peGFP-C3, only 0.024 mM of the same GAG is needed to start releasing peGFP-C3 from polyplexes prepared with *l*-PEI$_{20}$. This result shows that the branched structure of *b*-PEI$_{25}$ provides more stability to the polyplex and confers more protection to the DNA. Hence, *b*-PEI$_{25}$ chains appear to have a greater capacity for DNA condensation compared to *l*-PEI$_{20}$ [81] Our results are in good agreement with what was reported by Dai *et al.*, where DNA/PEI polyplexes prepared with *l*-PEI release all DNA in presence of a certain amount of negatively charged dextran sulfate chains, whereas DNA/PEI polyplexes prepared with *b*-PEI were more stable and did not release all DNA [82].

3.5. Thermodynamics of b-PEI/polyanions complexation

ITC analysis was used to investigate the complexation between *b*-PEI$_{25}$ and various biological polyanions (CT-DNA, HA, CS and HP) to better understand the thermodynamics of assembly and correlate this with the polyanions' ability to dissociate *b*-PEI$_{25}$/peGFP-C3 polyplexes. Fig. 13 shows the net differential enthalpies from the titration of the polyanions CT-DNA, HP, CS and HA by the *b*-PEI$_{25}$ in 100 mM HEPES buffer at pH 7.4. Clearly ITC curves are not simple sigmoids. Instead, two (or three) sequential processes are observed, as indicated by the presence of endothermic and exothermic peaks.

The addition of *b*-PEI$_{25}$ to CT-DNA, HP or CS, results in the formation of PECs through ion-pairing, an exothermic process that continues until charge equivalence is reached. Beyond this point, the further addition of *b*-PEI$_{25}$ triggers a structural rearrangement or partial dissociation of the polyplexes, accompanied by the release of water molecules. This rearrangement requires energy input, resulting in an endothermic effect, which is shown as a positive peak. Specifically, in Fig. 13a, the addition of *b*-PEI$_{25}$ into CT-DNA results in exothermic ion pairing up to a charge ratio of around R=0.5, at which an additional exothermic peak emerges. A closer examination of Fig. 3a suggests a slight shift in the conductivity slope around this charge ratio, although more measurement points would be necessary for definitive confirmation (Fig. S.I. 8). This shift can be attributed to the strong binding of the CT-DNA polyanion, which may raise the pK_a of *b*-PEI$_{25}$, leading greater protonation and, consequently, a higher enthalpy of electrostatic complexation. In contrast, the titration of *b*-PEI$_{25}$/HA (Fig. 13d) shows a purely endothermic profile, suggesting a weaker interaction between the two polyelectrolytes, a feature often

observed in coacervating systems [45]. Before interacting with the cationic charges of *b*-PEI_{25}, HA must undergo dehydration, an endothermic process. A slight additional endothermic peak around charge equivalence is observed before the heat exchange returns to zero.

The ITC results for all *b*-PEI_{25}/polyanions were analyzed using the MNIS model, which assumes that the overall heat exchange arises from the combined contributions observed during titration, as previously described [45-48]. Each contribution is characterized by a binding enthalpy ΔH, a binding constant *K* and a reaction stoichiometry noted *n*. Table 4 summarizes the parameters derived from these fits. The measured binding enthalpy for the ion-pairing process follows the order HP (-3.4 kJ/mol) > CT-DNA (-2.7 kJ/mol) > CS (-1.8 kJ/mol) > HA (+ 0.7 kJ/mol). This indicates that HP exhibits the strongest affinity for *b*-PEI_{25} and can effectively dissociate *b*-PEI_{25}/CT-DNA polyplexes, and thereby releasing DNA. However, as noted by Ma *et al.* in their study on DNA/chitosan complexation [20,83], titration experiments conducted in a buffer do not reflect the absolute enthalpy of complexation, as they include contributions from both the buffer's ionization state and that of the weak polycation, which in this case is *b*-PEI_{25}. Ma *et al.* also showed that the strong polyanionic nature of DNA allows the ionization of glucosamines of chitosan during complexation and is therefore responsible for proton transfer from the buffer to the polymer [20, 83]. However, since all our measurements were made in the same buffer, it was possible to compare the thermodynamic information for all polyanions between them in a relative way. A closer examination of the binding constant reveals that both $K_{1\text{-CT-DNA}}$ (2×10^6 M^{-1}) and $K_{1\text{-HP}}$ (0.8×10^6 M^{-1}) show similar, significantly higher values than $K_{1\text{-CS}}$ (1.3×10^5 M^{-1}) and $K_{1\text{-HA}}$ (2.7×10^4 M^{-1}) The lower binding constants for CS and HA are consistent with their inability to release DNA, while HP's higher constant reinforces its capacity to disassemble *b*-PEI_{25}/CT-DNA, and PEI/peGFP-C3 polyplexes. These findings are consistent with those reported by Ma *et al.*, who observed that HP, whose binding constant is similar to that of DNA, was capable of disrupting DNA/chitosan polyplexes [20].

4. Conclusions

It was demonstrated through conductimetric and ζ-potential measurements that electrostatic interaction between *b*-PEI$_{25}$ and polyanions in the absence of external salt is the main driving force behind polyplexes formation. Despite difference in charge density and structure between *b*-PEI$_{25}$ and polyanions, the effective complexation stoichiometry remains close to 1 for all systems. Polyplexes prepared at charge ratios ranging from 0.5 to 10 exhibits sizes smaller than 100 nm, with monomodal distributions and PDI below 0.30. AFM measurements suggest the existence of a complex hierarchical structure, where small primary polyplexes form during the initial stages of complexation and subsequently aggregate into larger secondary polyplex particles.

The formation of polyplexes from *b*-PEI$_{25}$ and plasmid DNA (peGFP-C3) was also studied, revealing no significant differences compared to polyplexes formed with linear DNA from calf-thymus. These polyplexes were exposed to varying amounts of GAGs, including heparin (HP), chondroitin sulfate (CS), and hyaluronic acid (HA). Among these, HP was the only GAG capable of disrupting *b*-PEI$_{25}$/peGFP-C3 polyplexes and releasing peGFP-C3. This is attributed to HP's high negative charge density, resulting from the presence of carboxylate groups and multiple sulfate groups in each disaccharide unit. The amount of heparin required to dissociate the PEI/peGFP-C3 polyplexes was found to scale linearly with the charge ratio. This indicates that heparin initially complexes stoichiometrically with the excess PEI in the polyplex suspension before displacing plasmid DNA withing the polyplexes. Notably, HP with Mw as low as 6.2 x 10^3 g/mol can displace plasmid DNA of 3.21 x10^6 g/mol, highlighting the critical role of the competitive polyanion's charge density. Furthermore, the branched structure of PEI was found to provide greater stability to polyplexes compared to its linear counterpart, likely due to its higher charge density.

Finally, ITC measurements further revealed that, HP exhibits the highest binding constant with *b*-PEI$_{25}$ among the GAGs tested, indicating its strongest affinity: K_{HP} (0.8 x 10^6 M^{-1}) > K_{CS} (1.3 x 10^5 M^{-1}) > K_{HA} (2.7 x 10^4 M^{-1}). This strong interaction enables HP to effectively dissociate the *b*-PEI$_{25}$/DNA polyplexes and release the DNA.

Acknowledgements

The authors of this work acknowledge Agnès Burel from Microscopy Rennes Imaging Center (MRic) of the UMS Biosit (FBI member, ANR-10-INBS-04), University of Rennes for TEM analysis, for TEM observations; Bertrand Lefeuvre from the Institut des Sciences Chimiques de Rennes for the Malvern Zetasizer NanoZS facilities, Boris Jacquette, from the "Soft Matter" platform of the IMMM laboratory at Le Mans University, where SEC measurements were partially carried out, and Marielle Blot, also for SEC measurements performed at the ISCR, Rennes. Paulina Alejandra Montaño González acknowledges CONAHCYT (CVU 770728), for the awarded scholarship, the Organic Polymer Chemistry Laboratory (LCPO, Bordeaux), the Centre de Recherche Paul Pascal (CRPP, Bordeaux) and the Institute of Chemical Sciences (ISCR) of Rennes for technical facilities to carry on the research. Lourdes Mónica Bravo-Anaya acknowledges the French National Agency of Research (ANR) for the grant (ANR-21-CE06-0027-01), the IEA P^{2}NanoBio founded by the CNRS, as well as the AES 2021 and the AIS Allocation 2023 founded by Rennes Métropole.

References

[1] R. Ni, R. Feng, Y. Chau, Synthetic approaches for nucleic acid delivery: choosing the right carriers, Life 9 (3) (2019) 1–28, https://doi.org/10.3390/life9030059.

[2] J.W. Salameh, L. Zhou, S.M. Ward, C.F. Santa Chalarca, T. Emrick, M.L. Figueiredo. Polymer-mediated gene therapy: Recent advances and merging of delivery techniques. Wiley Interdiscip Rev Nanomed Nanobiotechnol. 12(2) (2020) 1-23. https://doi.org/10.1002/wnan.1598.

[3] S. Berger, U. Lächelt, E. Wagne, Dynamic carriers for therapeutic RNA delivery, PNAS 121(11) (2024). https://doi.org/10.1073/pnas.2307799120

[4] L. M. Mollé, C. H. Smyth, D. Yuen, A. P. R. Johnston, Nanoparticles for vaccine and gene therapy: overcoming the barriers to nucleic acid delivery, WIREs Nanomed. Nanobi. 14 (6) (2022) e1809. https://doi.org/10.1002/wnan.1809.

[5] B. D. Monnery. Polycation-mediated transfection: mechanisms of internalization and intracellular trafficking, Biomacromolecules 22 (10) (2021) 4060–83. https://doi.org/10.1021/acs.biomac.1c00697.

[6] K. Ita, Polyplexes for gene and nucleic acid delivery: progress and bottlenecks, Eur. j. pharm. Sci. 150 (2020) 105358. https://doi.org/10.1016/j.ejps.2020.105358.

[7] M. D. Buschmann, A. Merzouki, M. Lavertu, M. Thibault, M. Jean, V. Darras, Chitosans for delivery of nucleic acids, Adv. Drug Deliv. Rev. 65 (9) (2013) 1234–70. https://doi.org/10.1016/j.addr.2013.07.005.

[8] K. Modra, S. Dai, H. Zhang, B. Shi, J. Bi. Polycation-mediated gene delivery: challenges and considerations for the process of plasmid DNA transfection, Eng. Life Sci. 15 (5) (2015) 489–98. https://doi.org/10.1002/elsc.201400043.

[9] I. Porello, N. Bono, F. Candiani, F. Cellesi , Advancing nucleic acid delivery through cationic polymer design: non-cationic building blocks from the toolbox, Polym. Chem. 15 (2024) 2800-2826. https://doi.org/10.1039/D4PY00234B

[10] P. Wu, H. Chen, R. Jin, T. Weng, J. K. Ho, C. You, L. Zhang, X. Wang, C. Han, Non-viral gene delivery systems for tissue repair and regeneration. J. Transl. Med. 16 (1) (2018) 1–20. https://doi.org/10.1186/s12967-018-1402-1.

[11] K. von Gersdorff, N. N. Sanders, R. Vandenbroucke, S. C. De Smedt, E. Wagner, M. Ogris, The internalization route resulting in successful gene expression depends on both cell line and polyethylenimine polyplex type, Mol. Ther. 14 (5) (2006) 745–753. https://doi.org/10.1016/j.ymthe.2006.07.006.

[12] J. Chen, X. Guan, Y. Hu, H. Tian, X. Chen, Peptide-based and polypeptide-based gene delivery systems. (2017). In: Cheng, Y. (eds) Polymeric Gene Delivery Systems. Topics in Current Chemistry Collections. Springer, Cham. https://doi.org/10.1007/978-3-319-77866-2_4.

[13] J. Nguyen, F. C. Szoka, Nucleic acid delivery: the missing pieces of the puzzle? Acc. Chem. Res. 45 (7) (2012) 1153–62. https://doi.org/10.1021/ar3000162.

[14] M. J. Mehta, H. J. Kim, S. B. Lim, M. Naito, K. Miyata, Recent Progress in the Endosomal Escape Mechanism and Chemical Structures of Polycations for Nucleic Acid Delivery, Macromolecular Bioscience, 24(4) (2024). https://doi.org/10.1002/mabi.202300366

[15] M. Durymanov, J. Reineke. Non-viral delivery of nucleic acids: insight into mechanisms of overcoming intracellular barriers, Front. Pharmacol. 9 (2018) 971–85. https://doi.org/10.3389/fphar.2018.00971.

[16] L. M. P. Vermeulen, S. C. De Smedt, K. Remaut, K. Braeckmans, The proton sponge hypothesis: fable or fact? Eur. J. Pharm. Biopharm. 129 (2018) 184–190. https://doi.org/10.1016/j.ejpb.2018.05.034.

[17] E. C. Freeman, L. M. Weiland, W. S. Meng, Modeling the proton sponge hypothesis: examining proton sponge effectiveness for enhancing intracellular gene delivery through multiscale modeling, J. Biomater. Sci. Polym. Ed. 24 (4), (2012) 398–416. https://doi.org/10.1080/09205063.2012.690282.

[15] A. D. Kulkarni, Y. H. Vanjari, K. H. Sancheti, H. M. Patel, V. S. Belgamwar, S. J. Surana, C. V. Pardeshi, Polyelectrolyte complexes: mechanisms, critical experimental aspects, and applications, Artif. Cells Nanomed. Biotechnol. 44 (7) (2016) 1615–1625. https://doi.org/10.3109/21691401.2015.1129624.

[16] S. Lankalapalli, V. R. M. Kolapalli, Polyelectrolyte complexes: a review of their applicability in drug delivery technology, Indian J. Pharm. Sci. 71 (5) (2009) 481–487. https://doi.org/10.4103/0250-474X.58165.

[17] D. Wu, L. Zhu, Y. Li, X. Zhang, S. Xu, G. Yang, T. Delair, Chitosan-based colloidal polyelectrolyte complexes for drug delivery: a review, Carbohydr. Polym. 238 (2020) 116126. https://doi.org/10.1016/j.carbpol.2020.116126.

[18] L. Leclercq, M. Boustta, M. Vert, Polymer degradation as a tool to study polyelectrolyte complex formation and stability, ACS Symp. Ser. 1114 (2012) 59–72. https://doi.org/10.1021/bk-2012-1114.ch005.

[19] K. Prydz, Determinants of glycosaminoglycan (GAG) structure, Biomolecules 5 (3) (2015) 2003–2022. https://doi.org/10.3390/biom5032003.

[20] P. L. Ma, M. Lavertu, F. M. Winnik, M. D. Buschmann, Stability and binding affinity of DNA/chitosan complexes by polyanion competition, Carbohydr. Polym. 176 (2017) 167–176. https://doi.org/10.1016/j.carbpol.2017.08.002

[21] P. Band, A. Lukton, Catalytic influence of heparin on auramine O hydrolysis: A basis for differentiating heparin from other glycosaminoglycans based on its properties as a polyelectrolyte, Biopolymers, 23 (1984) 2223-2241. https://doi.org/10.1002/bip.360231109

[22] L. M. Bravo-Anaya, J. F. A. Soltero, M. Rinaudo, DNA/chitosan electrostatic complex. Int. J. Biol. Macromol. 88 (2016) 345–53. https://doi.org/10.1016/j.ijbiomac.2016.03.035.

[23] L. M. Bravo-Anaya, K. G. Fernández Solís, J. Rosselgong, J. L. E. Nano Rodríguez, F. Carvajal, M. Rinaudo, Chitosan-DNA polyelectrolyte complex: influence of chitosan characteristics and mechanism of complex formation. Int. J. Biol. Macromol. 126 (2019) 1037–49. https://doi.org/10.1016/j.ijbiomac.2019.01.008.

[24] D.G. Mintis, T.S. Alexiou, and V.G. Mavrantzas, Effect of pH and Molecular Length on the Structure and Dynamics of Linear and Short-Chain Branched Poly(ethylene imine) in Dilute Solution: Scaling Laws from Detailed Molecular Dynamics. J.Phys. Chem. B 124(28) (2020) 6154–6169, https://doi.org/10.1021/acs.jpcb.0c04135

[25] K. Modra, S. Dai, H. Zhang, B. Shi, J. Bi, Polycation-mediated gene delivery: challenges and considerations for the process of plasmid DNA transfection, Eng. Life Sci. 15 (5) (2015) 489–98. https://doi.org/10.1002/elsc.201400043.

[26] Y.-K. Kim, C. Zhang, C.-S. Cho, M.-H. Cho, H.-L. Jiang, Poly (amino ester) s-based polymeric gene carriers in cancer gene therapy, in Novel Gene Therapy Approaches, (2013) 376–396 IntechOpen. https://doi.org/10.5772/54740.

[27] A. von Harpe, H. Petersen, Y. Li, T. Kissel, Characterization of commercially available and synthesized polyethylenimines for gene delivery, J. Control. Release 69 (2) (2000) 309–322. https://doi.org/10.1016/S0168-3659(00)00317-5.

[28] A. Hall, U. Lächelt, J. Bartek, E. Wagner, S. M. Moghimi, Polyplex evolution: understanding biology, optimizing performance, Molecular therapy 25 (7) (2017) 1476–91. https://doi.org/10.1016/j.ymthe.2017.01.024.

[29] X. Wang, D. Niu, C. Hu, P. Li, Polyethyleneimine-based nanocarriers for gene delivery, Curr. Pharm. Des. 21 (42), (2015) 6140–6156. https://doi.org/10.2174/1381612821666151027152907

[30] W. T. Godbey, K. K. Wu, A. G. Mikos, Size matters: molecular weight affects the efficiency of poly(ethylenimine) as a gene delivery vehicle, J. Biomed. Mater. Res. 45 (3) (1999) 268–75. https://doi.org/10.1002/(SICI)1097-4636(19990605)45:3<268::AID-JBM15>3.0.CO;2-Q

[31] T. Bieber, H. P. Elsässer. Preparation of a low molecular weight polyethylenimine for efficient cell transfection. BioTechniques 30 (1) (2001) 74–81. https://doi.org/10.2144/01301st03.

[32] S. Choosakoonkriang, B. A. Lobo, G. S. Koe, J. G. Koe, C. R. Middaugh, Biophysical characterization of PEI/DNA complexes, J. Pharm. Sci. 92 (8) (2003) 1710–22. https://doi.org/10.1002/jps.10437.

[33] M. Ruponen, S. Ylä-Herttuala, A. Urtti, Interactions of polymeric and liposomal gene delivery systems with extracellular glycosaminoglycans: physicochemical and transfection studies, BBA - Biomembranes 1415 (2) (1999) 331–41. https://doi.org/10.1016/S0005-2736(98)00199-0.

[34] M. Bertschinger, G. Backliwal, A. Schertenleib, M. Jordan, D. L. Hacker, F. M. Wurm, Disassembly of polyethylenimine-DNA particles in vitro: implications for polyethylenimine-mediated DNA delivery, J. Control. Release 116 (1) (2006) 96–104. https://doi.org/10.1016/j.jconrel.2006.09.006.

[35] Y. Wang, M. Ye, R. Xie, S. Gong, Enhancing the in vitro and in vivo stabilities of polymeric nucleic acid delivery nanosystems, Bioconjug. Chem. 30 (2) (2019) 325–37. https://doi.org/10.1021/acs.bioconjchem.8b00749.

[36] B. Abdallah, A. Hassan, C. Benoist, D. Goula, J. P. Behr, B. A. Demeneix, A powerful nonviral vector for in vivo gene transfer into the adult mammalian brain: polyethylenimine, Hum. Gene Ther. 7 (16) (1996) 1947–54. https://doi.org/10.1089/hum.1996.7.16-1947.

[37] U. Lungwitz, M. Breunig, T. Blunk, A. Göpferich, Polyethylenimine-based non-viral gene delivery systems, Eur. J. Biopharm. 60 (2) (2005) 247–66. https://doi.org/10.1016/j.ejpb.2004.11.011.

[38] J. Casper, S. H. Schenk, E. Parhizkar, P. Detampel, A. Dehshahri, J. Huwyler, Polyethylenimine (PEI) in gene therapy: Current status and clinical applications, J. Control. Release 362 (2023) 667–691. https://doi.org/10.1016/j.jconrel.2023.09.001.

[39] K. Kunath, A. von Harpe, D. Fischer, H. Petersen, U. Bickel, K. Voigt, T. Kissel, Low-molecular-weight polyethylenimine as a non-viral vector for DNA delivery: comparison of physicochemical properties, transfection efficiency and in vivo distribution with high-molecular-weight polyethylenimine, J. Control. Release 89 (1) (2003) 113–25. https://doi.org/10.1016/S0168-3659(03)00076-2.

[40] L. M. Bravo-Anaya, M. Rinaudo, F. A. Soltero Martínez, Conformation and rheological properties of calf-thymus DNA in solution, Polymers 8 (51), (2016) 1–19. https://doi.org/10.3390/polym8020051.

[41] C. Jreyssaty, Q. Shi, H. Wang, X. Qiu, F. M. Winnik, X. Zhang, K. Dai, M Benderdour, J. C. Fernandes, Efficient nonviral gene therapy using folate-targeted chitosan-DNA nanoparticles in vitro, Int. Sch. Res. Notices 1 (2012) 369270. https://doi.org/10.5402/2012/369270.

[42] C. J. B. van Treslong, A. J. Staverman, Poly (ethylenimine) II. Potentiometric titration behaviour in comparison with other weak polyelectrolytes, Recl. Trav. Chim. Pays-Bas 93 (6) (1974) 171–178. https://doi.org/10.1002/recl.19740930612.

[43] S. Bhattacharjee, DLS and zeta potential – What they are and what they are not? J. Control. Release 235 (2016) 337–351. https://doi.org/10.1016/j.jconrel.2016.06.017.

[44] L. Xu, F. Mallamace, Z. Yan, F. W. Starr, S. V. Buldyrev, H. E. Stanley, Appearance of a fractional Stokes-Einstein relation in water and a structural interpretation of its onset, Nat. Phys. 5 (2009) 565–569. https://doi.org/10.1038/nphys1328.

[45] P. Van der Meeren, M. Kasinos, H. Saveyn, Relevance of two-dimensional Brownian motion dynamics in applying nanoparticle tracking analysis, Methods Mol. Biol. 906 (2012) 511–524. https://doi.org/10.1007/978-1-61779-953-2_42.

[45] L. Vitorazi, N. Ould-Moussa, S. Sekar, J. Fresnais, W. Loh, J. P. Chapel, J. F. Berret, Evidence of a two-step process and pathway dependency in the thermodynamics of poly(diallyldimethylammonium chloride)/poly(sodium acrylate) complexation, Soft Matter 10 (2014) 9496–505. https://doi.org/10.1039/C4SM01461H.

[46] T. Delas, M. Mock-Joubert, J. Faivre, M. Hofmaier, O. Sandre, F. Dole, J.P. Chapel, A. Crépet, S. Trombotto, T. Delair, T., C. Schatz, Effects of Chain Length of Chitosan Oligosaccharides on Solution Properties and Complexation with siRNA. Polymers 11, (2019) 1-19. https://doi.org/10.3390/polym11081236

[47] M. M. Pierce, C. S. Raman, B. T. Nall, Isothermal titration calorimetry of protein–protein interactions, Methods 19 (2) (1999) 213–221. https://doi.org/10.1006/meth.1999.0852.

[48] T. Wiseman, S. Williston, J. F. Brandts, L. N. Lin, Rapid measurement of binding constants and heats of binding using a new titration calorimeter, Anal. Biochem. 179 (1) (1989) 131–137. https://doi.org/10.1016/0003-2697(89)90213-3.

[49] R. L. Cleland, J. L. Wang, D. M. Detweiler, Polyelectrolyte properties of sodium hyaluronate. 2. Potentiometric titration of hyaluronic acid, Macromolecules 15 (2) (1982) 386–395. https://doi.org/10.1021/ma00230a037.

[50] M. Bathe, G. C. Rutledge, A. J. Grodzinsky, B. Tidor, A coarse-grained molecular model for glycosaminoglycans: application to chondroitin, chondroitin sulfate, and hyaluronic acid, Biophys. J. 88 (6) (2005) 3870–3887. https://doi.org/10.1529/biophysj.104.058800.

[51] B. Casu, U. Gennaro, A conductimetric method for the determination of sulfate and carboxyl groups in heparin and other mucopolysaccharides, Carbohydr. Res. 39 (1), (1975) 168–176. https://doi.org/10.1016/s0008-6215(00)82654-3.

[52] Z. Shriver, I. Capila, G. Venkataraman, R. Sasisekharan, Heparin and heparan sulfate: analyzing structure and microheterogeneity, Handb. Exp. Pharmacol. 207 (2012) 159–176. https://doi.org/10.1007/978-3-642-23056-1_8.

[53] T. Miller, M. C. Goude, T. C. McDevitt, J. S. Temenoff, Molecular engineering of glycosaminoglycan chemistry for biomolecule delivery, Acta Biomater. 10 (4) (2014) 1705–1719. https://doi.org/10.1016/j.actbio.2013.09.039.

[54] P. Vicennati, A. Giuliano, G. Ortaggi, A. Masotti, Polyethylenimine in medicinal chemistry, Curr. Med. Chem. 15 (2008) 2826–2839. https://doi.org/10.2174/ 092986708786242778.

[55] K. Grenda, A. Idström, L. Evenäs, M. Persson, K. Holmberg, R. Bordes, An analytical approach to elucidate the architecture of polyethyleneimines, Journal of Applied Polymer Science, 139(7) (2022). 1-7. http://dx.doi.org/10.1002/app.51657

[56] G.J.M. Koper, M. Borkovec, Proton binding by linear, branched, and hyperbranched polyelectrolytes, Polymer, 51(24) (2010) 5649-5662 https://doi.org/10.1016/j.polymer.2010.08.067.

[57] H. Kodama, T. Miyajima, M. Mori, M. Takahashi, H. Nishimura and S. Ishiguro, A unified analytical treatment of the acid-dissociation equilibria of weakly acidic linear polyelectrolytes and the conjugate acids of weakly basic linear polyelectrolytes, 275 (1997) 938–945. https://doi.org/10.1007/s003960050169

[58] C.E. Gallops, C. Yu, J.D. Ziebarth, Y. Wang, Effect of the Protonation Level and Ionic Strength on the Structure of Linear Polyethyleneimine, ACS Omega 4 (2019) 7255−7264. https://doi.org/10.1021/acsomega.9b00066.

[59] Z. Ou and M. Muthukumara, Entropy and enthalpy of polyelectrolyte complexation: Langevin dynamics Simulations, J Chem Phys. 124(15) (2006) 154902. https://doi.org/10.1063/1.2178803

[60] L. Webster, M. B. Huglin, I. D. Robb, Complex formation between polyelectrolytes in dilute aqueous solution, Polymer 38 (6) (1997) 1373–1380. https://doi.org/10.1016/S0032-3861(96)00650-7.

[61] G. S. Manning, Molecular theory of polyelectrolyte solutions with applications to electrostatic properties of polynucleotides, Q. Rev. Biophys. 11 (2) (1978) 179–246. https://doi.org/10.1017/S0033583500002031

[62] D. Matulis, I Rouzina, V. A. Bloomfield, Thermodynamics of DNA binding and condensation: isothermal titration calorimetry and electrostatic mechanism, J. Mol. Biol. 296 (4) (2000) 1053–1063. https://doi.org/10.1006/jmbi.1999.3470.

[63] D.P. Mascotti, T.M. Lohman, Thermodynamic Extent of Counterion Release Upon Binding Oligolysines to Single-Stranded Nucleic Acids, Proceedings of the National Academy of Sciences of the United States of America, 87, (1990), 3142-3146. https://doi.org/10.1073/pnas.87.8.3142.

[64] Q. Wang, J. B. Schlenoff, The Polyelectrolyte Complex/Coacervate Continuum Macromolecules, 47(9) (2014) 3108–3116. https://doi.org/10.1021/ma500500q

[65] L. M. Bravo-Anaya, B. Garbay, J. L. E. Nando-Rodríguez, F. Carvajal Ramos, E. Ibarboure, K. Bathany, Y. Xia, J. Rosselgong, G. Joucla, E. Garanger, S. Lecommandoux, Nucleic acids complexation with cationic elastin-like polypeptides: stoichiometry and stability of nano-assemblies, J. Colloid Interface Sci. 557 (2019) 777–792. https://doi.org/10.1016/j.jcis.2019.09.054.

[66] M. Alatorre-Meda, P. Taboada, B. Krajewska, M. Willemeit, A. Deml, R. Klösel, J. R. Rodríguez, DNA–poly(diallyldimethylammonium chloride) complexation and transfection efficiency, J. Phys. Chem. B 114 (2010) 9356–9366. https://doi.org/10.1021/jp1016856.

[67] L. M. Bravo-Anaya, J. Rosselgong, K. G. Fernández-Solís, Y. Xiao, A. Vax, E. Ibarboure, A. Ruban, C. Lebleu, G. Joucla, B. Garbay, E. Garanger, S. Lecommandoux, Coupling of RAFT polymerization and chemoselective post-modifications of elastin-like polypeptides for the synthesis of gene delivery hybrid vectors, Polym. Chem. 12, (2021) 226–241. https://doi.org/10.1039/D0PY01293A.

[68] A.S. Michaels, L. Mir, and N.S. Schneider, A Conductometric Study of Polycation-Polyanion Reactions in Dilute Aqueous Solution, J. Phys. Chem. 69,5 (1965) 1447–1455. https://doi.org/10.1021/j100889a003

[69] F. Amaduzzi, F. Bomboi, A. Bonincontro, F. Bordi, S. Casciardi, L. Chronopoulou, M. Diociaiuti, F. Mura, C. Palocci, S. Sennato, Chitosan–DNA complexes: charge inversion and DNA condensation, Colloid Surf. B 114 (2014) 1–10. https://doi.org/10.1016/j.colsurfb.2013.09.029.

[70] C. W. Frevert, T. N. Wight, Extracellular matrix : matrix proteoglycans, in Encyclopedia of Respiratory Medicine, ed. G. J. Laurent and S. D. Shapiro, Academic Press, Oxford, 2006, pp. 184–188. https://doi.org/10.1016/B0-12-370879-6/00150-2.

[71] A. V. Kabanov, V. A. Kabanov, Interpolyelectrolyte and block ionomer complexes for gene delivery: physico-chemical aspects, Adv. Drug Deliv. Rev. 30 (1998) 49–60. https://doi.org/10.1016/S0169-409X(97)00106-3.

[72] F. Cousin, J. Gummel, D. Ung, F. Boué, Polyelectrolyte-protein complexes: structure and conformation of each specie revealed by SANS, Langmuir 21 (21) (2005) 9675–9688. https://doi.org/10.1021/la0510174.

[73] I. Konko. Aqueous solutions of complexes formed by model polyelectrolytes of opposite charges. Doctoral Dissertation, University of Strasbourg, Alsace, France, 2015.

[74] N. Jemili, M. Fauquignon, E. Grau, N. Fatin-Rouge, F. Dole, J.-P. Chapel, W. Essafi, C. Schatz, Complexation in Aqueous Solution of a Hydrophobic Polyanion (PSSNa) Bearing Different Charge Densities with a Hydrophilic Polycation (PDADMAC), Polymers 14 (12) (2022), 1-22. https://doi.org/10.3390/polym14122404

[75] M. Haddou. Complexes de polyélectrolytes: morphologies, cinétique et thermodynamique d'assemblage. Doctoral Dissertation, University of Bordeaux, Aquitaine, France, 2019.

[76] D. Gilot, M-L. Miramon, T. Benvegnu, V. Ferrieres, O. Loreal, C. Guguen-Guillouzo, D. Plusquellec, P. Loyer. Cationic lipids derived from glycine betaine promote efficient and non-toxic gene transfection in cultured hepatocytes. J Gene Med. 4 (4) (2002) 415-27. doi: 10.1002/jgm.279.

[77] A.A. Gurtovenko, Molecular-Level Insight into the Interactions of DNA/Polycation Complexes with Model Cell Membranes. J Phys Chem B. 1 123(30) (2019) 6505-6514. doi: 10.1021/acs.jpcb.9b05110.

[78] F. Coelho, C. Botelho, J.L. Paris, E.F. Marques and B.F.B. Silva, Influence of the media ionic strength on the formation and in vitro biological performance of polycation-DNA complexes, J. Mol. Liq. 344 (2021) 1-10, https://doi.org/10.1016/j.molliq.2021.117930.

[79] M. Ruponen, P. Honkakoski, S. Rönkkö, J. Pelkonen, M. Tammi, A. Urtti, Extracellular and Intracellular Barriers in Non-Viral Gene Delivery, J. Control. Release 93 (2) (2003) 213–17. https://doi.org/10.1016/j.jconrel.2003.08.004.

[80] I. Moret, J. E. Peris, V. M. Guillem, M. Benet, F. Revert, F. Dasí, A. Crespo, S. F. Aliño, Stability of PEI-DNA and DOTAP-DNA complexes: effect of alkaline PH, heparin and serum, J. Control. Release 76 (1–2) (2001) 169–181. https://doi.org/10.1016/S0168-3659(01)00415-1.

[81] Diana Costa, Artur J.M. Valente, João A. Queiroz, Ângela Sousa, Finding the ideal polyethylenimine-plasmid DNA system for co-delivery of payloads in cancer therapy, Colloids and Surfaces B: Biointerfaces 170 (2018) 627–636, https://doi.org/10.1016/j.colsurfb.2018.06.063

[82] Z. Dai, T. Gjetting, M. A. Mattebjerg, C. Wu, T.L. Andresen, Elucidating the interplay between DNA-condensing and free polycations in gene transfection through a mechanistic study of linear and branched PEI, Biomaterials, 32(33) (2011) 8626-8634, https://doi.org/10.1016/j.biomaterials.2011.07.044.

[83] P.L. Ma, M. Lavertu, F.M. Winnik, M.D. Buschmann, New insights into chitosan-DNA interactions using isothermal titration microcalorimetry. Biomacromolecules 10(6) (2009) 1490-1499. https://doi.org/10.1021/bm900097s

Captions

Fig. 1.- Chemical structures of GAGs (sodium form). a) heparin (Γ_M = 3.2), b) chondroitin 4-sulfate (Γ_M = 1.5) and c) sodium hyaluronate (Γ_M = 0.7). Γ_M corresponds to the Manning parameter, $\Gamma_M = l_B/b$, where l_B is the Bjerrum length, corresponding to the length at which the Coulombic potential between two-unit charges is equal to the thermal energy. In an aqueous solution, the Bjerrum length is typically taken as 7.1 Å. b_i represents the average distance between two ionized sites along the polymer chain, including carboxylate and sulfate groups, assuming full ionization at pH 7.4. A polyelectrolyte is considered weakly charged if $\Gamma_M < 1$ and highly charged if $\Gamma_M > 1$ [20]. Data of average axial periodicity (nm/disaccharide) and sulfate/hexoseamine ratio are taken from Band et al. [21].

Fig. 2.- Chemical structures of a) linear and b) branched PEI (Γ_M = 1.2 for *l*-PEI and *b*-PEI for 50% of protonation) [20,24].

Fig. 3.- Variation in conductivity as a function of the charge ratio (R=[+]/[-]) during the titration of the polyanion with *b*-PEI_{25}. a) *b*-PEI_{25}/CT-DNA, b) *b*-PEI_{25}/HP, c) *b*-PEI_{25}/CS and d) *b*-PEI_{25}/HA. Measurements were performed at 25 °C. $C_{CT\text{-}DNA}$ = 0.03 mg/mL, C_{HP} = 0.01 mg/mL, C_{CS} = 0.03 mg/mL and C_{HA} = 0.01 mg/mL, were prepared with water. $C_{b\text{-}PEI25}$ = 0.94 mg/mL for CT-DNA, HP and CS and 0.47 mg/mL for HA. Both *b*-PEI_{25} solutions were prepared with water and were adjusted at pH 7.4 before use. Conductivity titrations were performed in duplicate and data averaged.

Fig. 4.- ζ–potential measurements as a function of the charge ratio ([+]/[-]) during the formation of polyplexes. a) *b*-PEI_{25}/CT-DNA, b) *b*-PEI_{25}/HP, c) *b*-PEI_{25}/CS and d) *b*-PEI_{25}/HA. The *b*-PEI_{25} solution, prepared with water and adjusted at pH 7.4, was gradually added to the polyanion solution. The same experimental conditions as described in Fig. 3 were applied. ζ–potential measurements were performed in triplicate and the whole titrations were performed in duplicate. For CS and HP, the concentration of negative charged groups used in the calculations of R was determined from the equivalence obtained in conductimetric titrations.

Fig. 5.- Intensity-averaged size distribution obtained by DLS for polyplexes prepared at various charge ratios, R = 0.5, 0.8, 3, 5, 10. a) *b*-PEI_{25}/CT-DNA, b) *b*-PEI_{25}/HP, c) *b*-PEI_{25}/CS and d) *b*-

PEI_{25}/HA. All polyanions were prepared in water at a concentration of 0.034 mg/mL. The *b*-PEI_{25} solution was prepared in water at a concentration of 0.034 mg/mL and the pH adjusted at 7.4. Polyplexes were prepared by adding *b*-PEI_{25} to the polyanion in one-shot and then vortexing. DLS measurements were performed in duplicate.

Fig. 6.- AFM images of polyplexes prepared at R = 4. a) *b*-PEI_{25}/CT-DNA, b) *b*-PEI_{25}/HP, c) *b*-PEI_{25} /CS, d) *b*-PEI_{25}/HA. Polyplexes were prepared in water through one-shot mixing of PEI with polyanions, then diluting them 1:100 with milliQ water.

Fig. 7.- a) ζ-potential measurements as a function of $[N^+]/[P^-]$ ratio during *b*-PEI_{25}/peGFP-C3 polyplexes formation (PEI was added dropwise to the plasmid solution). b) Electrophoresis gel assays showing the effect of charge ratio, $[N^+]/[P^-]$, on the electrophoretic mobility of peGFP-C3 plasmid. M represents the apparent electrophoretic mobility of the DNA markers (SmartLadder MW-1700-10 Eurogentec). c) Intensity-averaged size distribution obtained by DLS for polyplexes prepared at R= 3, 5, 10 and 15. d) TEM images of *b*-PEI_{25}/peGFP-C3 polyplexes prepared at a charge ratio of $[N^+]/[P^-]$= 10. e) AFM images of *b*-PEI_{25}/eGFP-C3 polyplexes prepared at a charge ratio of $[N^+]/[P^-]$= 4. $C_{peGFP\text{-}C3}$ = 0.034 mg/mL and $C_{b\text{-}PEI25}$= 0.94 mg/mL, both prepared in water and the pH adjusted to 7.4 for *b*-PEI_{25}. ζ-potential experiments were performed in triplicate. DLS measurements were performed in duplicate. For DLS, TEM, AFM analysis, *b*-PEI_{25}/peGFP-C3 polyplexes were prepared through rapid one-shot mixing of *b*-PEI_{25} to peGFP-C3 plasmid.

Fig. 8.- Electrophoresis gel assays showing the effect of increasing concentration of a) HP, b) CS and c) HA, on the release of peGFP-C3 plasmid from *b*-PEI_{25}/peGFP-C3 polyplexes prepared at R= 4. The concentrations of GAGs are given in negative charges based on their chemical composition and conductimetric titrations. M represents the apparent electrophoretic mobility of the DNA markers (SmartLadder MW-1700-10 Eurogentec) and (G) the polyanion alone using the highest concentration. The mass concentrations of polymers and charged repetitive units in the polyplexes formed at R = 4 are: $C_{peGFP\text{-}C3}$ = 0.005 mg/mL (0.015 mM in water) and $C_{b\text{-}PEI25}$= 0.0235 mg/mL (0.164 mM at pH 7.4 with 30% of protonation).

Fig. 9.- Electrophoresis gel assays showing the effect of increasing charge concentration of heparin on the electrophoretic mobility of peGFP-C3 plasmid from *b*-PEI_{25}/peGFP-C3

polyplexes prepared at a) R= 3, b) R= 5, c) R= 9 and d) R= 14. M represents the apparent electrophoretic mobility of the DNA markers (SmartLadder MW-1700-10 Eurogentec). The experimental concentrations of peGFP-C3 and *b*-PEI_{25} are similar to those used in Fig. 7.

Fig. 10.- Heparin concentration (in terms of negatively charged groups) required to induce partial and complete dissociation of *b*-PEI_{25}/peGFP-C3 polyplexes as a function of charge ratio ($[N^+]/[P^-]$). $C_{peGFP\text{-}C3}$ = 0.05 mg/mL prepared in water and $C_{b\text{-}PEI25}$= 0.0235 mg/mL in water (pH 7.4). The black line corresponds to the linear fit for the complete dissociation results (R^2= 0.9949).

Fig. 11.- Electrophoresis gel assays showing the effect of heparin molecular weight: a) HP-Por with a Mw of 33 610 g/mol, and b) HP with a MW of 6 211 g/mol, on the electrophoretic mobility of peGFP-C3 plasmid from *b*-PEI_{25}/peGFP-C3 polyplexes prepared at R= 4. M represents the apparent electrophoretic mobility of the DNA markers (SmartLadder MW-1700-10 Eurogentec). The experimental concentrations of peGFP-C3 and *b*-PEI_{25} are similar to those used in Fig. 7.

Fig. 12.- Electrophoresis gel assays showing the effect of PEI structure: a) linear PEI and b) branched PEI, on the electrophoretic mobility of peGFP-C3 plasmid from *l*-PEI_{20}/peGFP-C3 and *b*-PEI_{25}/peGFP-C3 polyplexes, respectively, prepared at R= 4. M represents the apparent electrophoretic mobility of the DNA markers (SmartLadder MW-1700-10 Eurogentec). $C_{peGFP\text{-}C3}$ = 0.05 mg/mL prepared in water, $C_{l\text{-}PEI20}$= 0.0247 mg/mL and $C_{b\text{-}PEI25}$= 0.0235 mg/mL, both PEI solutions adjusted to pH 7.4.

Fig. 13.- Integrated data obtained from titration of *b*-PEI_{25} in 100 mM HEPES buffer at pH 7.4 into a) CT-DNA, b) HP, c) CS, and d) HA. $C_{CT\text{-}DNA}$ = 0.333 mg/mL (1.01 mM), C_{HP} = 0.322 mg/mL (1.79 mM), C_{CS} = 0.426 mg/mL (1.82 mM), C_{HA} = 0.385 mg/mL (0.96 mM) and $C_{b\text{-}PEI25}$ = 1.118 mg/mL (26 mM in total repetitive units, 7.8 mM in protonated units at pH 7.4). The solid red line corresponds to the fits using the modified multiple non-interacting sites (MNIS) model [45-47]. The charge ratio was calculated taking into account 40 % protonation of *b*-PEI_{25} in 100 mM buffer (vs. 30% in water) [42].

Tables

Table 1.- Characterization of GAGs by SEC-MALS.

Table 2.- Characterization of *b*-PEI_{25}/polyanions polyplexes by DLS, NTA (for R=5) and ζ-potential.

Table 3.- Characterization of *b*-PEI_{25}/peGFP-C3 prepared by "one shot and vortex" method with DLS, TEM, AFM and ζ-potential at different charge ratios.

Table 4.- Thermodynamic parameters obtained from the complexation between *b*-PEI_{25}/polyanions in 100 mM HEPES buffer at pH 7.4: primary (index 1), secondary (index 2) and tertiary (index 3) (for CT-DNA) processes obtained from the adjustment of the ITC curves with the modified multiple non-interacting sites (MNIS) model. ΔH, corresponding to the binding enthalpy, *K* to the binding constant and *n* denoting the stoichiometry.

Fig. 1.

International Journal of Biological Macromolecules

Paulina Alejandra Montaño-González, Lizeth Montserrat Bravo-Lozano, Soizic Chevance, François Dole, Julien Rosselgong, Pascal Loyer, Sylvain Tranchimand, Jean-Paul Chapel, Fabienne Gauffre, Christophe Schatz, Lourdes Mónica Bravo-Anaya

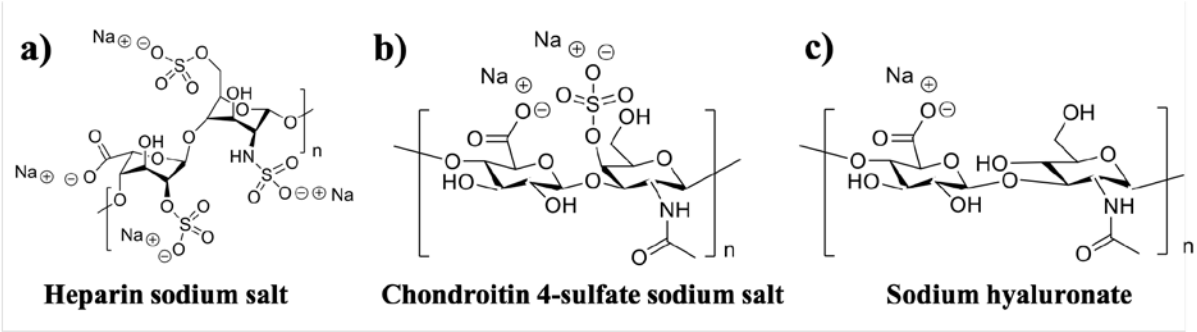

Fig. 2.

International Journal of Biological Macromolecules

Paulina Alejandra Montaño-González, Lizeth Montserrat Bravo-Lozano, Soizic Chevance, François Dole, Julien Rosselgong, Pascal Loyer, Sylvain Tranchimand, Jean-Paul Chapel, Fabienne Gauffre, Christophe Schatz, Lourdes Mónica Bravo-Anaya

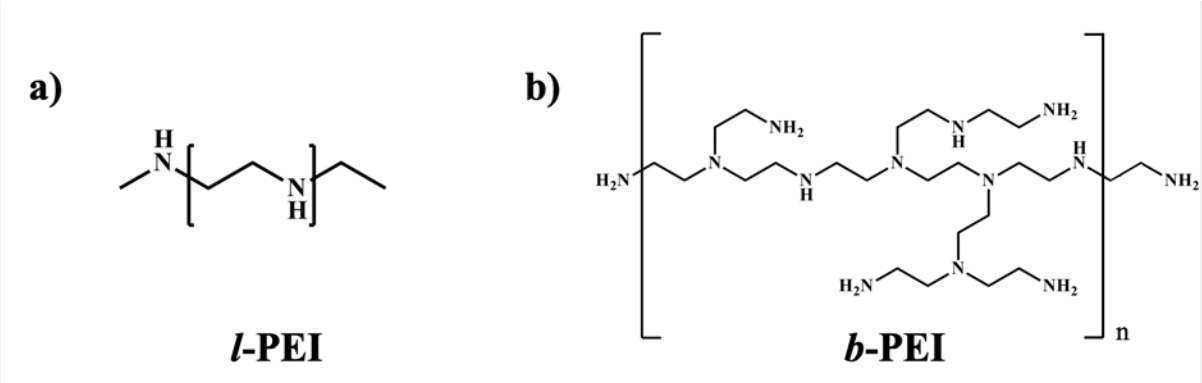

Fig. 3.

International Journal of Biological Macromolecules

Paulina Alejandra Montaño-González, Lizeth Montserrat Bravo-Lozano, Soizic Chevance, François Dole, Julien Rosselgong, Pascal Loyer, Sylvain Tranchimand, Jean-Paul Chapel, Fabienne Gauffre, Christophe Schatz, Lourdes Mónica Bravo-Anaya

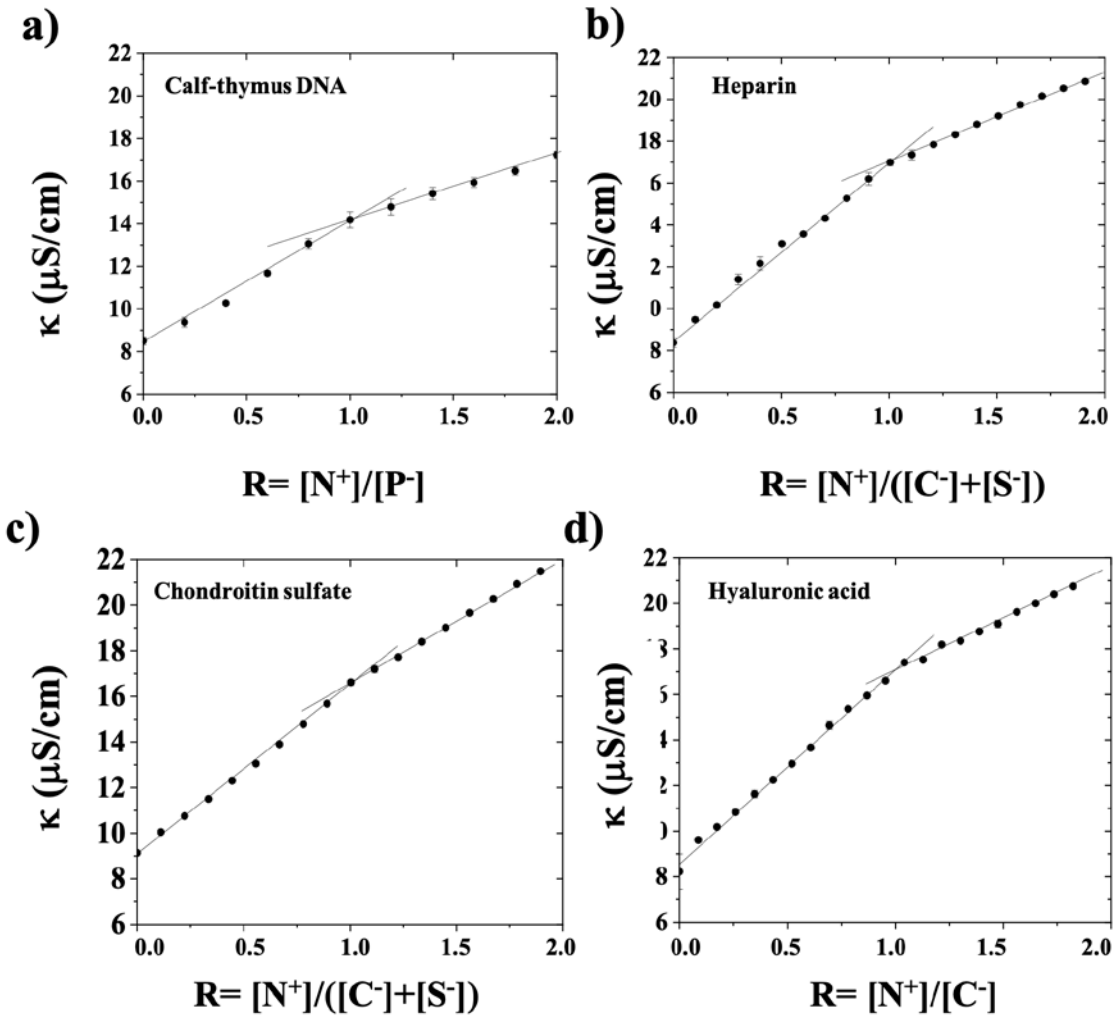

Fig. 4.

International Journal of Biological Macromolecules

Paulina Alejandra Montaño-González, Lizeth Montserrat Bravo-Lozano, Soizic Chevance, François Dole, Julien Rosselgong, Pascal Loyer, Sylvain Tranchimand, Jean-Paul Chapel, Fabienne Gauffre, Christophe Schatz, Lourdes Mónica Bravo-Anaya

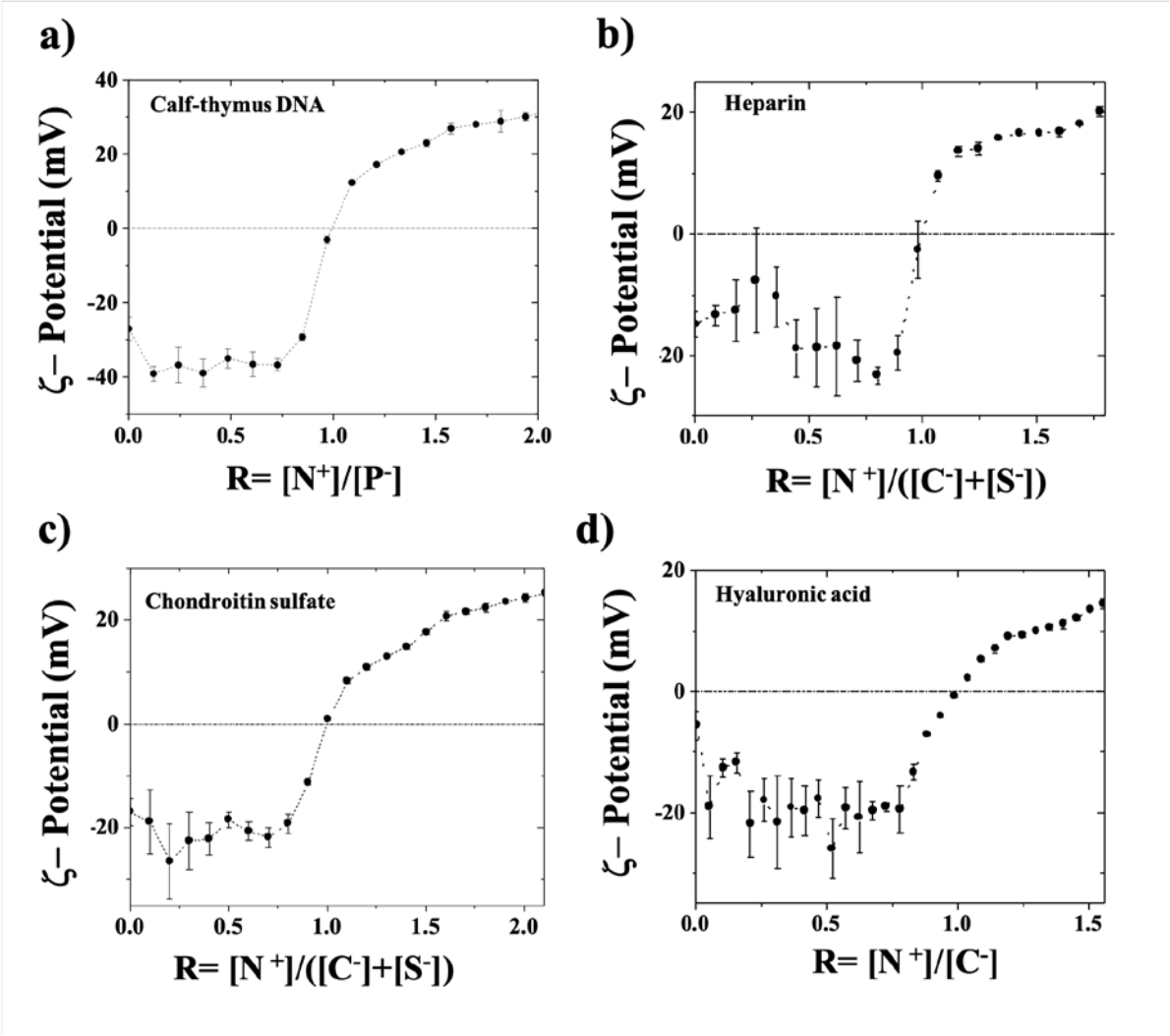

Fig. 5.

International Journal of Biological Macromolecules

Paulina Alejandra Montaño-González, Lizeth Montserrat Bravo-Lozano, Soizic Chevance, François Dole, Julien Rosselgong, Pascal Loyer, Sylvain Tranchimand, Jean-Paul Chapel, Fabienne Gauffre, Christophe Schatz, Lourdes Mónica Bravo-Anaya

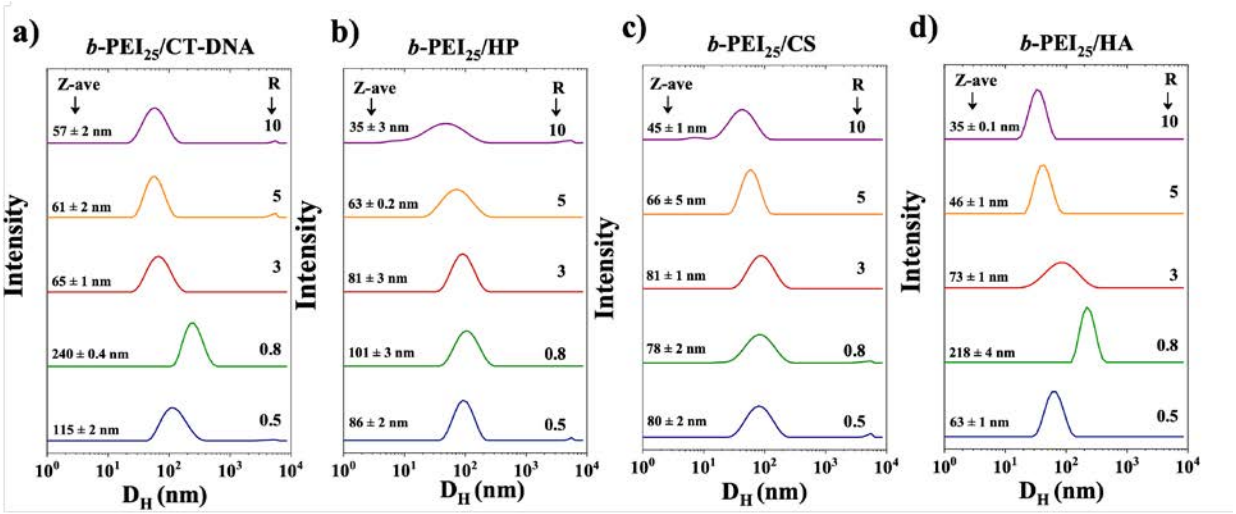

Fig. 6.

International Journal of Biological Macromolecules

Paulina Alejandra Montaño-González, Lizeth Montserrat Bravo-Lozano, Soizic Chevance, François Dole, Julien Rosselgong, Pascal Loyer, Sylvain Tranchimand, Jean-Paul Chapel, Fabienne Gauffre, Christophe Schatz, Lourdes Mónica Bravo-Anaya

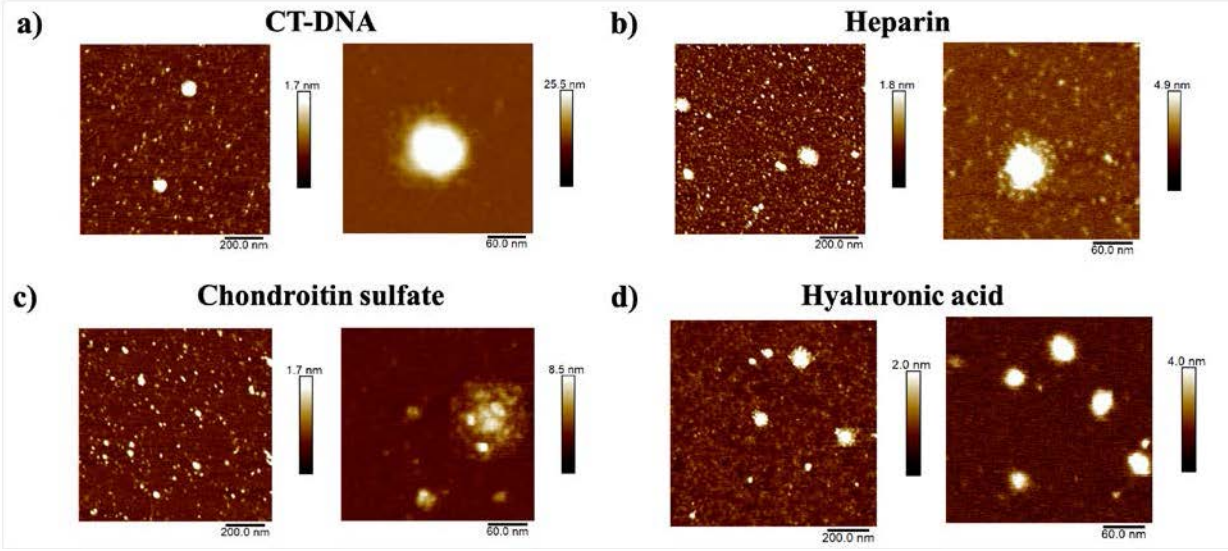

Fig. 7.

International Journal of Biological Macromolecules

Paulina Alejandra Montaño-González, Lizeth Montserrat Bravo-Lozano, Soizic Chevance, François Dole, Julien Rosselgong, Pascal Loyer, Sylvain Tranchimand, Jean-Paul Chapel, Fabienne Gauffre, Christophe Schatz, Lourdes Mónica Bravo-Anaya

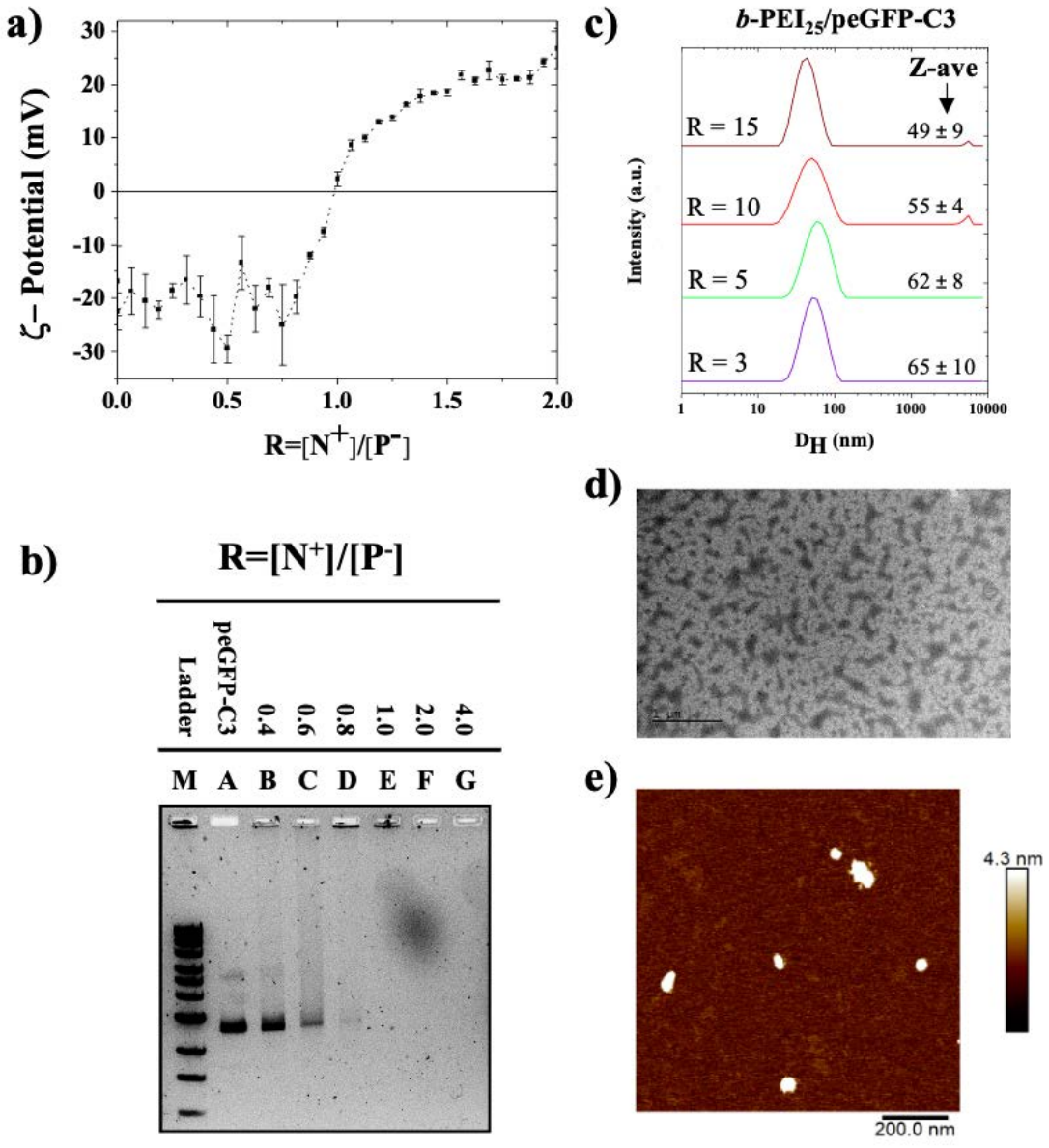

Fig. 8.

International Journal of Biological Macromolecules

Paulina Alejandra Montaño-González, Lizeth Montserrat Bravo-Lozano, Soizic Chevance, François Dole, Julien Rosselgong, Pascal Loyer, Sylvain Tranchimand, Jean-Paul Chapel, Fabienne Gauffre, Christophe Schatz, Lourdes Mónica Bravo-Anaya

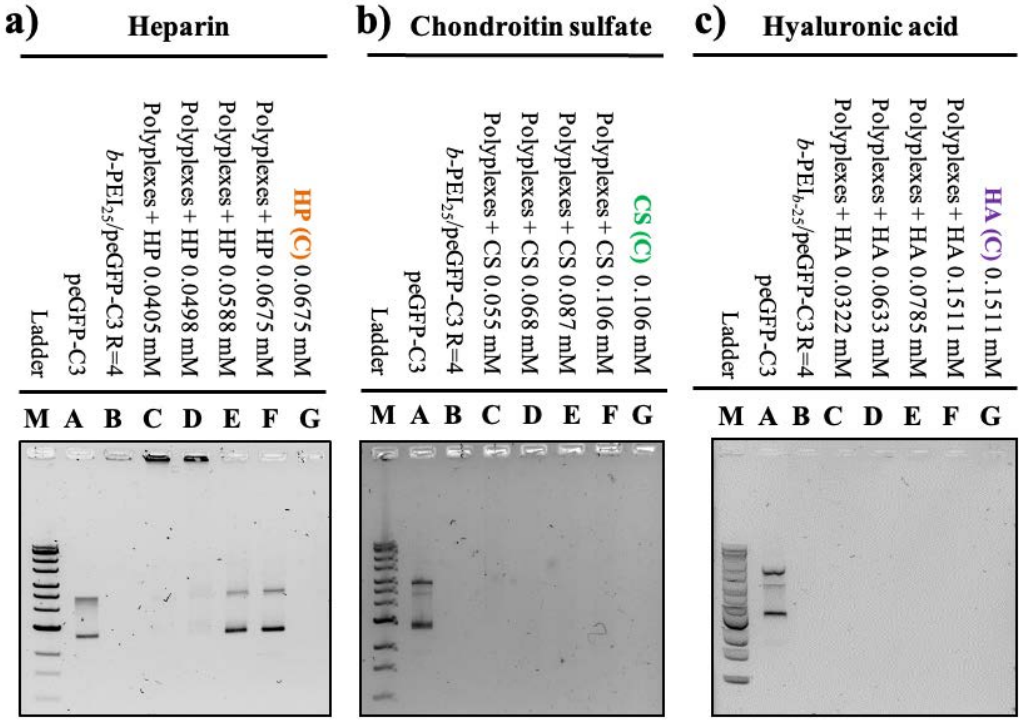

Fig. 9.

International Journal of Biological Macromolecules

Paulina Alejandra Montaño-González, Lizeth Montserrat Bravo-Lozano, Soizic Chevance, François Dole, Julien Rosselgong, Pascal Loyer, Sylvain Tranchimand, Jean-Paul Chapel, Fabienne Gauffre, Christophe Schatz, Lourdes Mónica Bravo-Anaya

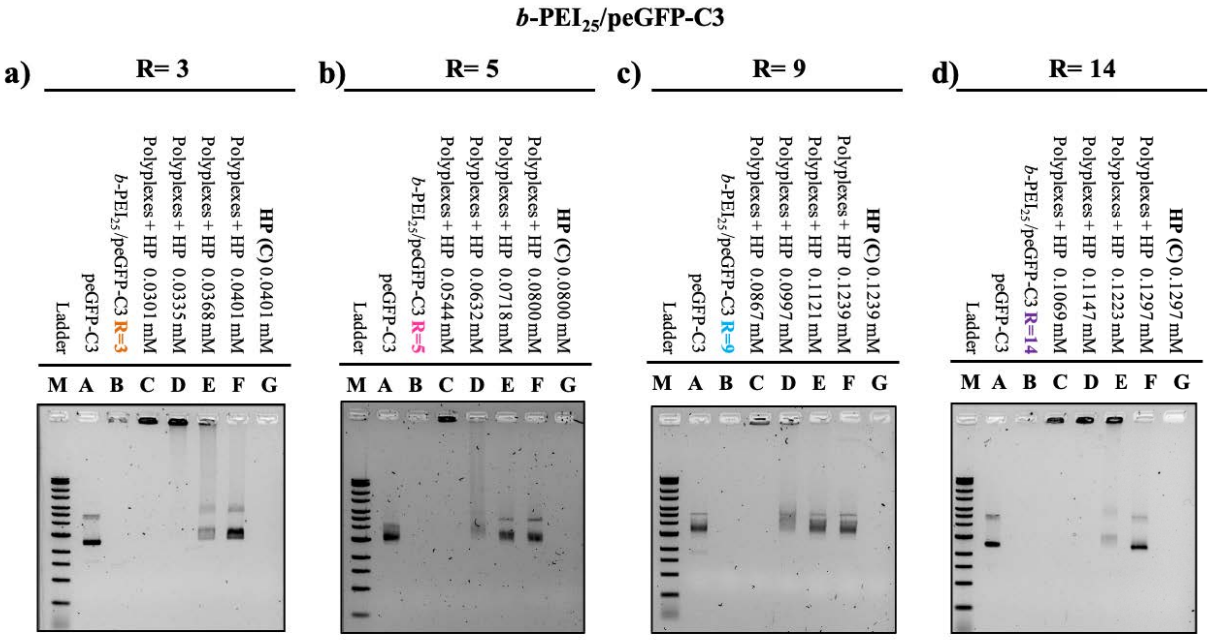

Fig. 10.

International Journal of Biological Macromolecules

Paulina Alejandra Montaño-González, Lizeth Montserrat Bravo-Lozano, Soizic Chevance, François Dole, Julien Rosselgong, Pascal Loyer, Sylvain Tranchimand, Jean-Paul Chapel, Fabienne Gauffre, Christophe Schatz, Lourdes Mónica Bravo-Anaya

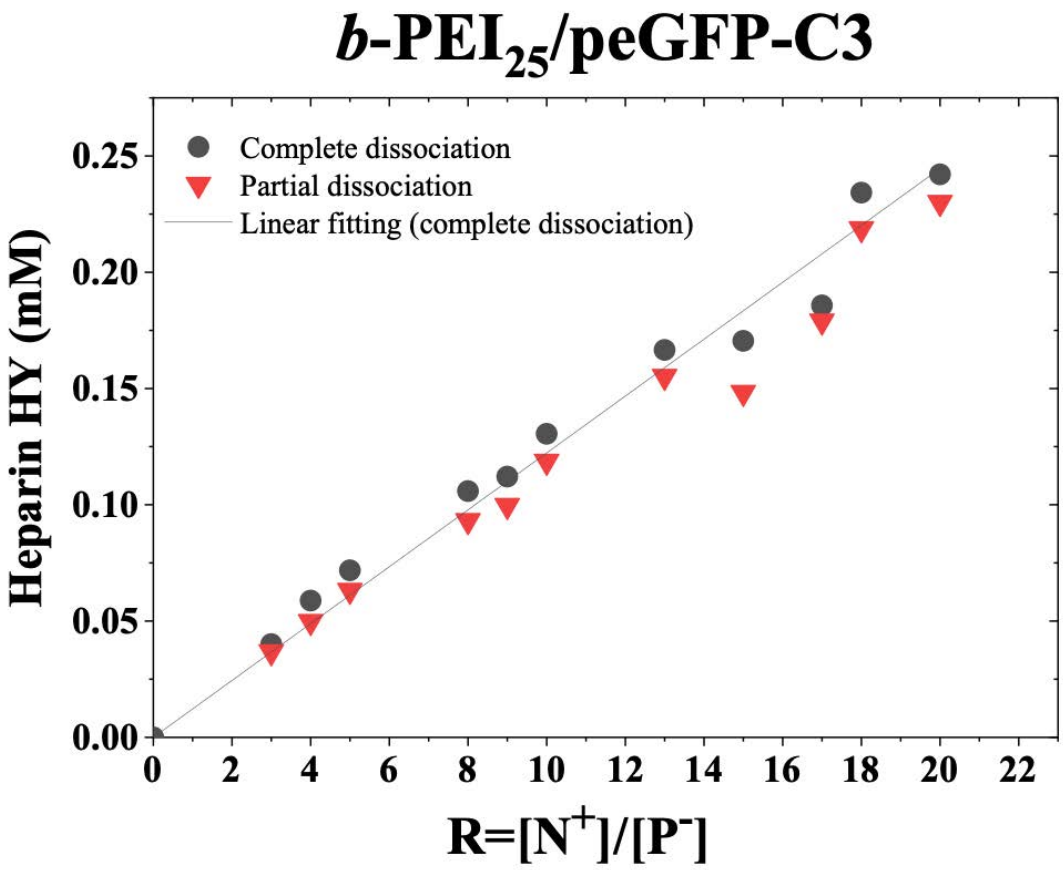

Fig. 11.

International Journal of Biological Macromolecules

Paulina Alejandra Montaño-González, Lizeth Montserrat Bravo-Lozano, Soizic Chevance, François Dole, Julien Rosselgong, Pascal Loyer, Sylvain Tranchimand, Jean-Paul Chapel, Fabienne Gauffre, Christophe Schatz, Lourdes Mónica Bravo-Anaya

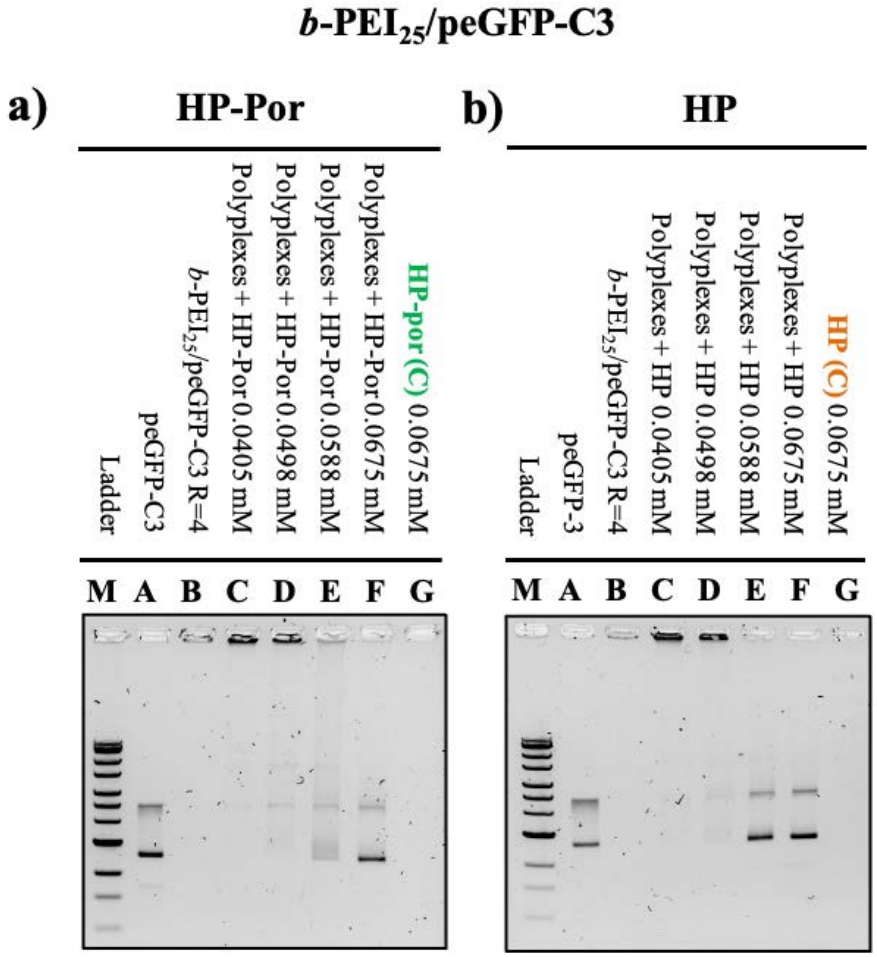

Fig. 12.

International Journal of Biological Macromolecules

Paulina Alejandra Montaño-González, Lizeth Montserrat Bravo-Lozano, Soizic Chevance, François Dole, Julien Rosselgong, Pascal Loyer, Sylvain Tranchimand, Jean-Paul Chapel, Fabienne Gauffre, Christophe Schatz, Lourdes Mónica Bravo-Anaya

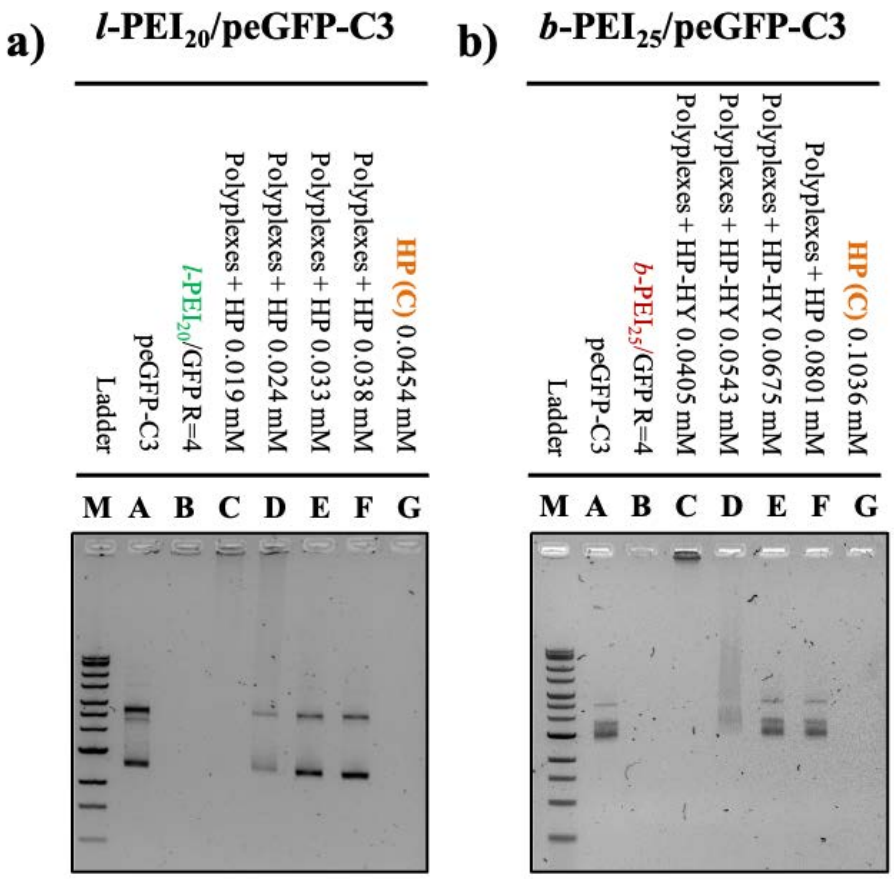

Fig. 13.

International Journal of Biological Macromolecules

Paulina Alejandra Montaño-González, Lizeth Montserrat Bravo-Lozano, Soizic Chevance, François Dole, Julien Rosselgong, Pascal Loyer, Sylvain Tranchimand, Jean-Paul Chapel, Fabienne Gauffre, Christophe Schatz, Lourdes Mónica Bravo-Anaya

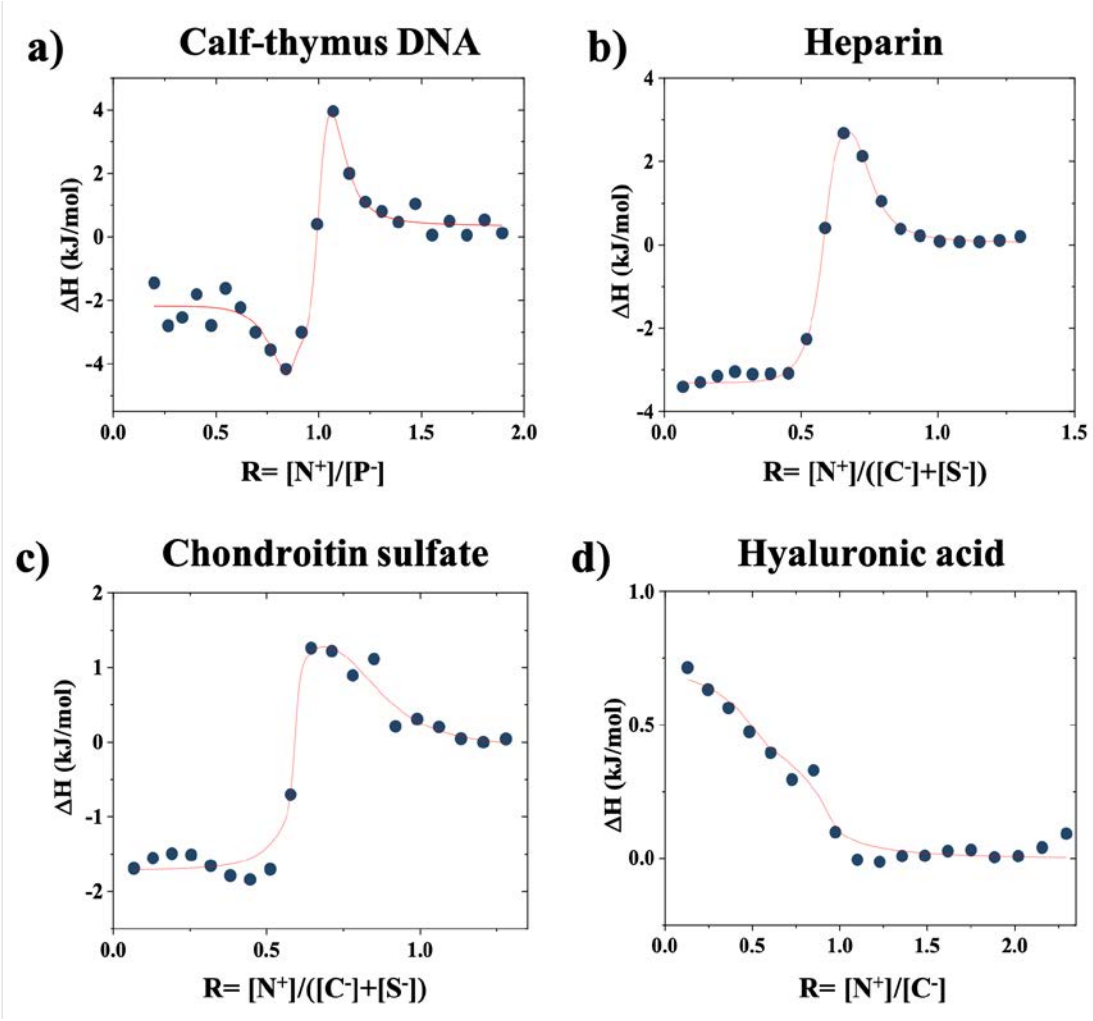

Table 1.

International Journal of Biological Macromolecules

Paulina Alejandra Montaño-González, Lizeth Montserrat Bravo-Lozano, Soizic Chevance, François Dole, Julien Rosselgong, Pascal Loyer, Sylvain Tranchimand, Jean-Paul Chapel, Fabienne Gauffre, Christophe Schatz, Lourdes Mónica Bravo-Anaya

Biological polyanion	**Mw[a] (g/mol)**	**Mn[b] (g/mol)**	***Đ*[c]**
Chondroitin Sulfate (CS)	5.6×10^4	2.5×10^4	2.298
Heparin (HP)	6.2×10^3	4.9×10^3	1.269
Heparin (HP-POR)	3.4×10^4	1.8×10^4	1.836
Hyaluronic Acid (HA)	1.5×10^6	1.2×10^6	1.225

[a] weight-average molar mass

[b] number-average molar mass

[c] dispersity (M_w/M_n)

Table 2.

International Journal of Biological Macromolecules

Paulina Alejandra Montaño-González, Lizeth Montserrat Bravo-Lozano, Soizic Chevance, François Dole, Julien Rosselgong, Pascal Loyer, Sylvain Tranchimand, Jean-Paul Chapel, Fabienne Gauffre, Christophe Schatz, Lourdes Mónica Bravo-Anaya

Biological polyanion	**R = [+]/[-]**	**D_H (nm) by DLS ***	**PDI**	**D_H (nm) by NTA ****	**ζ-potential (mV)**
Calf-thymus DNA (CT-DNA)	0.5	115 ± 2	0.17 ± 0.010		- 15.1 ± 0.9
	0.8	240 ± 1	0.11 ± 0.012		- 12.5 ± 0.8
	3	65 ± 1	0.19 ± 0.005		+ 30.2 ± 7.2
	5	61 ± 2	0.23 ± 0.077	68 ± 2	+ 30.4 ± 8.0
	10	57 ± 2	0.25 ± 0.012		+ 32.7 ± 6.4
Heparin (HP)	0.5	86 ± 2	0.26 ± 0.028		- 31.8 ± 4.7
	0.8	101 ± 3	0.13 ± 0.005		- 35.8 ± 1.2
	3	81 ± 3	0.15 ± 0.011		+ 31.9 ± 4.9
	5	66 ± 5	0.21 ± 0.006	72 ± 2	+ 35.9 ± 2.3
	10	45 ± 1	0.41± 0.029		+ 34.9 ± 4.0
Chondroitin Sulfate (CS)	0.5	80 ± 2	0.27 ± 0.029		- 23.5 ± 10.2
	0.8	78 ± 2	0.23 ± 0.013		- 17.2 ± 6.9
	3	81 ± 1	0.17 ± 0.001		+ 25.6 ± 0.9
	5	66 ± 5	0.21 ± 0.003	68 ± 5	+ 24.4 ± 1.9
	10	45 ± 1	-		+ 27.7 ± 1.4
Hyaluronic Acid (HA)	0.5	63 ± 1	0.14 ± 0.031		- 13.5 ± 1.7
	0.8	218 ± 4	0.03 ± 0.004		- 2.4 ± 0.4
	3	73 ± 1	0.20 ± 0.014		+ 26.2 ± 4.4
	5	46 ± 1	0.26 ± 0.006	53 ± 4	+ 27.6 ± 9.7
	10	35 ± 3	-		+ 26.2 ± 5.7

** by applying cumulant method*

*** at R= 5*

Table 3.

International Journal of Biological Macromolecules

Paulina Alejandra Montaño-González, Lizeth Montserrat Bravo-Lozano, Soizic Chevance, François Dole, Julien Rosselgong, Pascal Loyer, Sylvain Tranchimand, Jean-Paul Chapel, Fabienne Gauffre, Christophe Schatz, Lourdes Mónica Bravo-Anaya

Charge ratio	**D_H (nm) by DLS**	**PDI**	**Apparent diameter by AFM (nm) (for R=4)**	**Apparent diameter by TEM (nm) (for R=10)**	**ζ-potential (mV)**
3	65 ± 10	0.25 ± 0.03			+ 36 ± 2
5	62 ± 8	0.31 ± 0.05	42 ± 1	41 ± 13	+ 37 ± 1
10	55 ± 4	0.29 ± 0.01			+ 38 ± 3
15	49 ± 9	0.21 ± 0.06			+ 39 ± 5

Table 4.

International Journal of Biological Macromolecules

Paulina Alejandra Montaño-González, Lizeth Montserrat Bravo-Lozano, Soizic Chevance, François Dole, Julien Rosselgong, Pascal Loyer, Sylvain Tranchimand, Jean-Paul Chapel, Fabienne Gauffre, Christophe Schatz, Lourdes Mónica Bravo-Anaya

Biological polyanion	**ΔH_1 (kJ/mol)**	**K_1 (M^{-1})**	**n_1 (M^{-1})**
Calf-thymus DNA	-2.7	2.0×10^6	0.9
Hyaluronic Acid	+ 0.7	2.7×10^4	0.5
Chondroitin Sulfate	-1.8	1.3×10^5	0.6
Heparin	-3.4	0.8×10^6	0.6
	ΔH_2 (kJ/mol)	**K_2 (M^{-1})**	**n_2 (M^{-1})**
Calf-thymus DNA	-7.1	2.0×10^6	1.03
Hyaluronic Acid	+ 0.1	7.0×10^5	0.95
Chondroitin Sulfate	+ 2.2	4.0×10^3	0.82
Heparin	+ 4.4	1.8×10^5	0.75
	ΔH_3 (kJ/mol)	**K_3 (M^{-1})**	**n_3 (M^{-1})**
Calf-thymus DNA	+8.3	4.0×10^5	1.1

Author version of article published in *International Journal of Biological Macromolecules* 301 (2025) 140351

Interactions between PEI and biological polyanions and the ability of glycosaminoglycans in destabilizing PEI/peGFP-C3 polyplexes for genetic material release

Paulina Alejandra Montaño-González[a], Lizeth Montserrat Bravo-Lozano[b], Soizic Chevance[a], François Dole[c], Julien Rosselgong[a], Pascal Loyer[d], Sylvain Tranchimand[e], Jean-Paul Chapel[c], Fabienne Gauffre[a], Christophe Schatz[f], Lourdes Mónica Bravo-Anaya[a]*

[a] Univ Rennes, CNRS, ISCR (Institut des Sciences Chimiques de Rennes), UMR 6226, F-35000 Rennes, France

[b] Universidad de Guadalajara, CUCEI, Marcelino García Barragán 1421, CP 44430, Guadalajara, Jalisco, México

[c] Centre de Recherche Paul Pascal (CRPP), UMR CNRS 5031, Université de Bordeaux, 33600 Pessac, France

[d] Univ Rennes, Inserm, INRAE, Institut NUMECAN, UMR-A 1341, UMR-S 1317, Plateforme SynNanoVect, F-35000 Rennes, France

[e] Univ Rennes, École Nationale Supérieure de Chimie de Rennes, CNRS, ISCR, UMR 6226, F-35000 Rennes, France

[f] Univ Bordeaux, Bordeaux INP, LCPO, CNRS, UMR 5629, F-33000 Pessac, France

Corresponding author:

* Dr. Lourdes Mónica Bravo-Anaya, Email : lourdes-monica.anaya@univ-rennes.fr , Tel: +33-656-886-206.

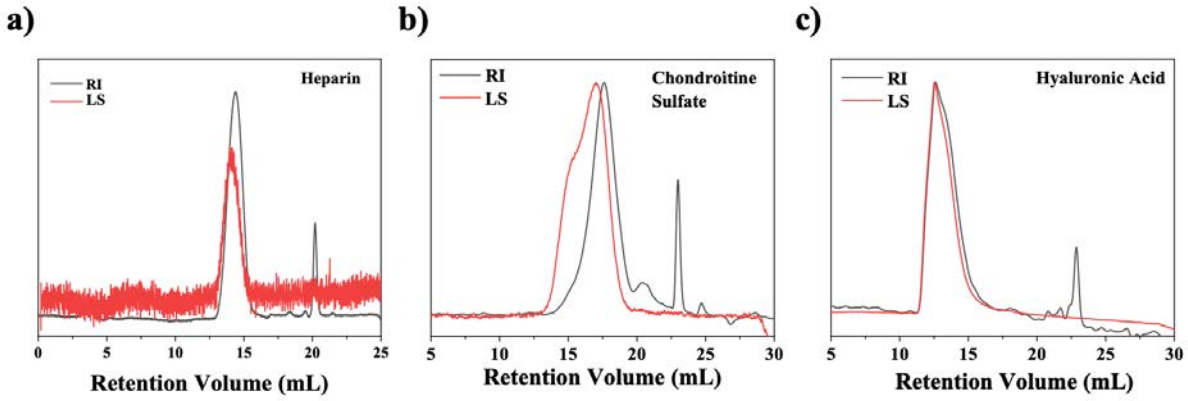

Fig. S.I. 1.- Size exclusion chromatograms in $NaNO_3$ 0.1M, NaN_3 for: a) HP, b) CS and c) HA, taken with refractive index and light scattering detectors. Measurement temperature: 25 °C.

One can observe that peaks obtained for CS in panel (b) do not fully overlap. This effect is a straightforward consequence of the polymer's dispersity, as analyzed by SEC using dual light scattering (LS) and differential refractive index (dRI) detection. No technical issues arise from the volume delay between the two detectors, as this parameter was accurately determined using low-dispersity polymer standards (Đ < 1.1). The observed shift between the chromatograms of the two detectors reflects the respective sensitivities of LS and dRI detection: LS measures the intensity of scattered light, which is strongly influenced by the molecular weight of the analyte. dRI measures the refractive index difference between the solvent and the analyte. It is proportional to the concentration of all solutes, regardless of molecular weight.

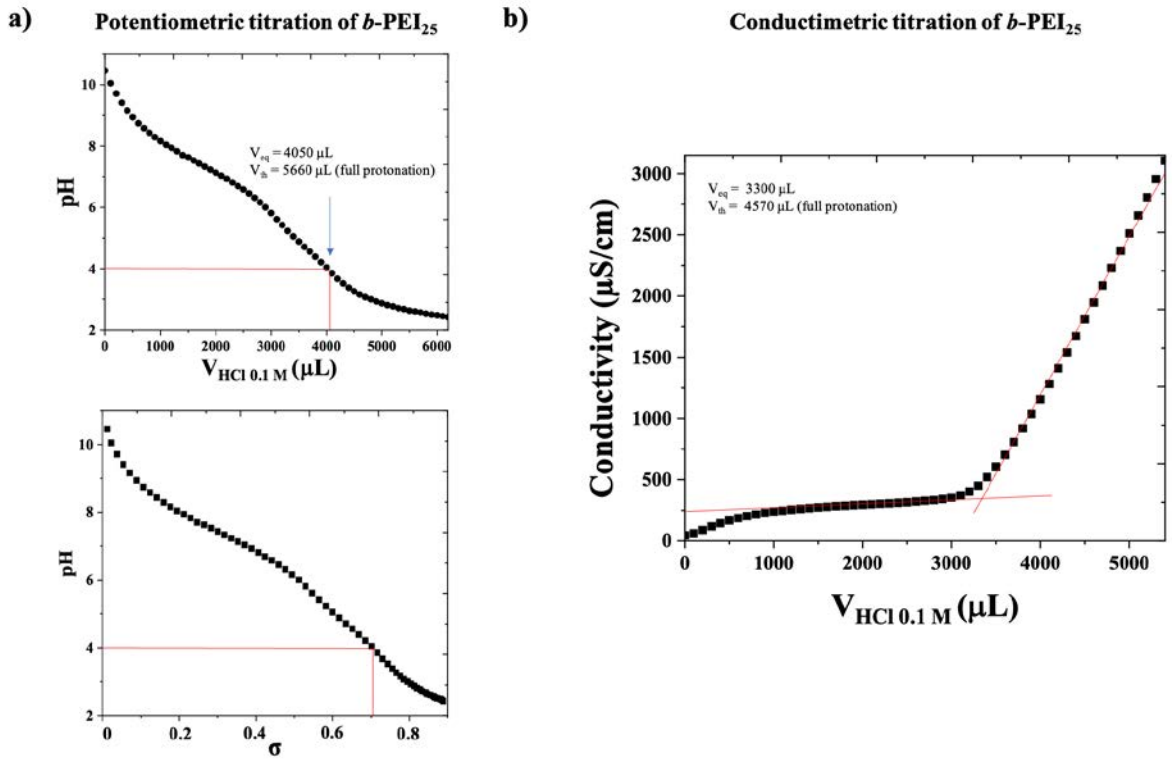

Fig. S.I. 2.- a) Potentiometric titration of a *b*-PEI_{25} solution at 1 mg/mL (23 mM) with HCl 0.1 M at 25°C. V_{th} and V_{eq} correspond to the theoretical volume to titrate all amine groups in the polymer and V_{eq} is the experimental volume obtained at equivalency. From these data, the pH variation as function of the protonation rate (σ) can be plotted. b) Conductimetric titration of a *b*-PEI_{25} solution at 1 mg/mL (23 mM) with HCl 0.1 M) at 25°C. Both titration methods highlight a maximal protonation rate of ~ 70%.

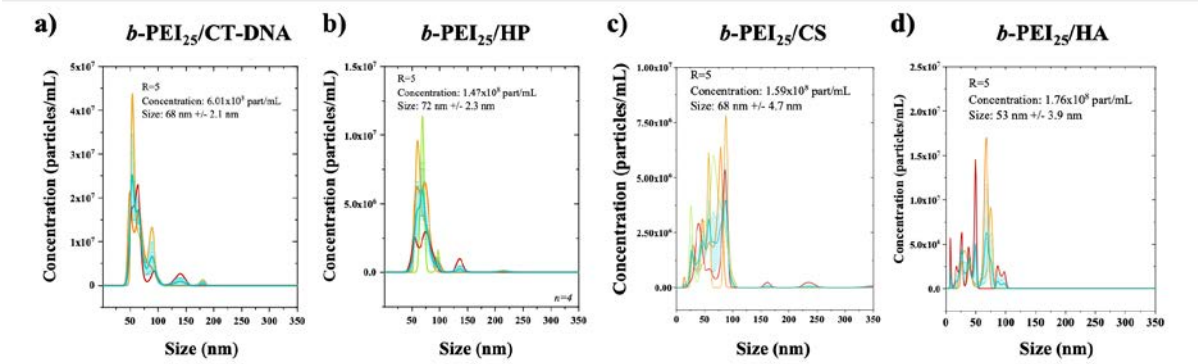

Fig. S.I. 3. NTA measurements for a) *b*-PEI_{25}/CT-DNA, b) *b*-PEI_{25}/HP, c) *b*-PEI_{25}/CS and d) *b*-PEI_{25}/HA polyplexes. All polyanions were prepared in water at a concentration of 0.034 mg/mL. $C_{b\text{-}PEI25}$ = 0.034 mg/mL in water (pH 7.4). DLS measurements were performed for polyplexes in duplicate. Polyplexes were prepared by adding *b*-PEI_{25} to the polyanion in one-shot and then vortexing.

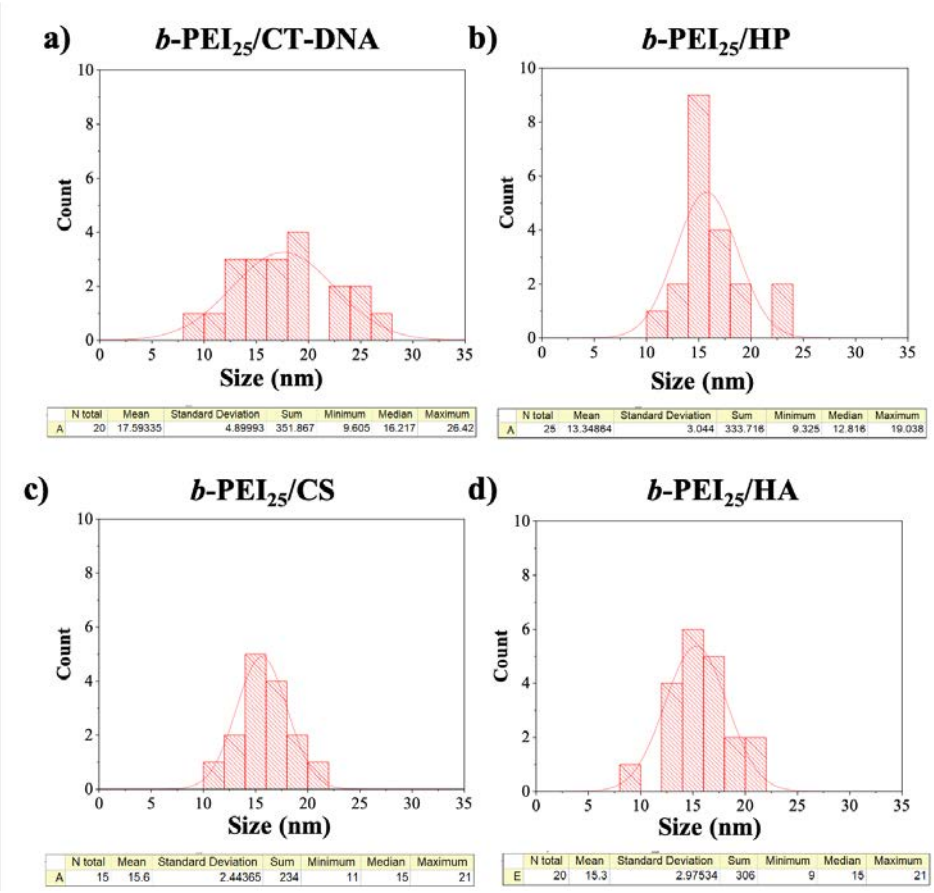

Fig. S.I. 4.- Size distribution obtained from AFM images analyzed with the ImageJ Software of a) *b*-PEI_{25}/CT-DNA, b) *b*-PEI_{25}/HP, c) *b*-PEI_{25}/CS and d) *b*-PEI_{25}/HA polyplexes prepared at a charge ratio of $[N^+]/[P^-]= 4$, focusing solely on primary polyplexes.

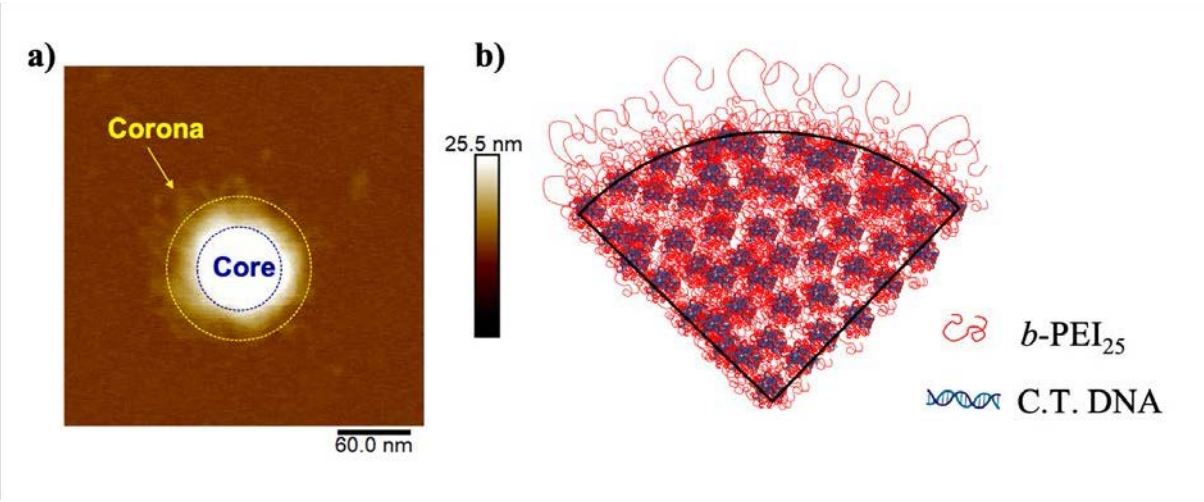

Fig. S.I. 5.- a) AFM images of *b*-PEI_{25}/peGFP-C3 polyplexes prepared at a charge ratio of $[N^+]/[P^-]$= 4. $C_{peGFP\text{-}C3}$ = 0.034 mg/mL in water and $C_{b\text{-}PEI\ 25\ kg/mol}$ = 0.94 mg/mL in water (pH 7.4). Polyplexes were prepared through rapid one-shot mixing of cationic PEI to anionic polyanions and then diluted 1/100 with milliQ water. b) Schematic representation of the hierarchical structure of polyplexes.

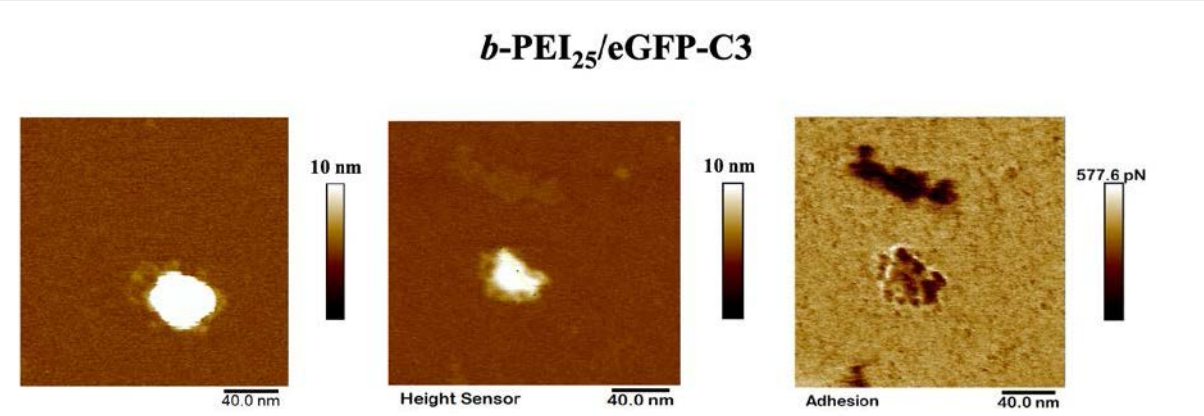

Fig. S.I. 6.- AFM images of *b*-PEI_{25}/peGFP-C3 polyplexes prepared at a charge ratio of $[N^+]/[P^-]$= 4. $C_{peGFP\text{-}C3}$ = 0.034 mg/mL in water and $C_{b\text{-}PEI\ 25\ kg/mol}$ = 0.94 mg/mL in water (pH 7.4). Polyplexes were prepared through rapid one-shot mixing of cationic PEI to anionic polyanions and then diluted 1/100 with milliQ water.

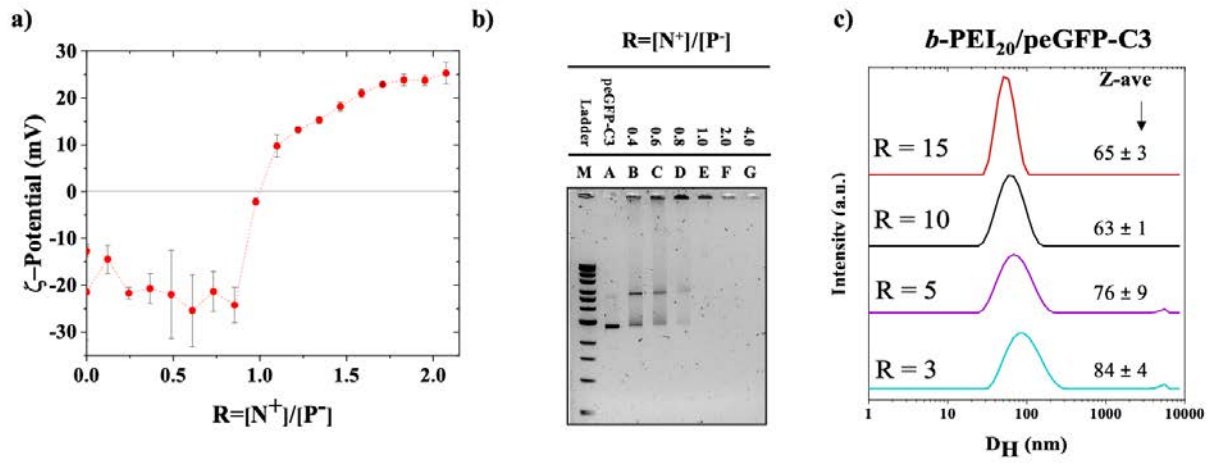

Fig. S.I. 7.- a) ζ-potential measurements as a function of $[N^+]/[P^-]$ ratio during *l*-PEI_{20}/peGFP-C3 polyplexes formation (where PEI was added dropwise to the plasmid solution). Similar to *b*-PEI_{25}/peGFP-C3 polyplexes, the effective complexation stoichiometry of *l*-PEI_{20}/peGFP-C3 polyplexes is close to 1, indicating that *l*-PEI_{20} achieves complete complexation at R=1. b) Electrophoresis gel assays showing the impact of the charge ratio, $[N^+]/[P^-]$, on the electrophoretic mobility of peGFP-C3 plasmid. It can be observed that *l*-PEI_{20} effectively complexes with peGFP-C3 at a charge ratio $[N^+]/[P^-]$=1, in good agreement with ζ-potential measurements. c) Intensity-averaged size distribution obtained by DLS for *l*-PEI_{20}/peGFP-C3 polyplexes prepared at R= 3, 5, 10 and 15 using the "one shot and vortex" methodology. Polyplexes present hydrodynamic sizes below 100 nm, with a monomodal distribution and PDI values below 0.3.

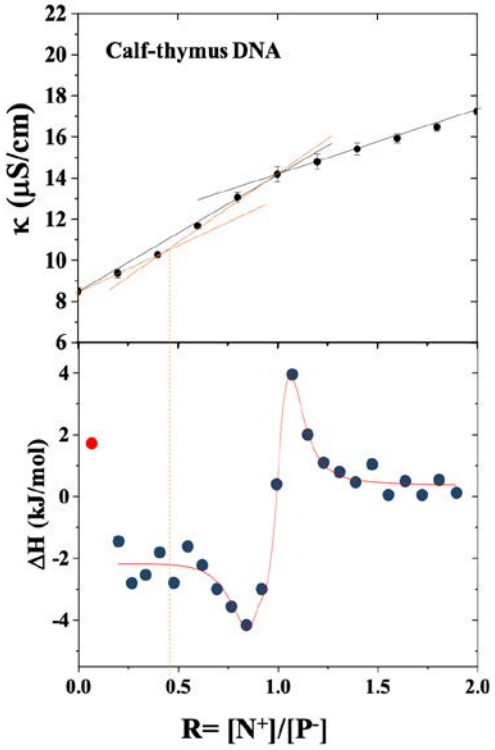

Fig. S.I. 8.- Variation in conductivity as a function of the charge ratio (R=[+]/[-]) during the titration of CT-DNA with *b*-PEI$_{25}$. Measurements were performed at 25 °C. $C_{CT\text{-}DNA}$ = 0.03 mg/mL in water. $C_{b\text{-}PEI25}$ = 0.94 mg/mL (pH 7.4). Integrated data obtained from titration of *b*-PEI$_{25}$ in 100 mM HEPES buffer at pH 7.4 into CT-DNA. $C_{CT\text{-}DNA}$ = 0.333 mg/mL (1.01 mM) and $C_{b\text{-}PEI25}$ = 1.118 mg/mL (26 mM in total repetitive units, 7.8 mM in protonated units at pH 7.4).

Table S.I. 1. Characterization of large b-PEI_{25}/polyanions secondary polyplexes (R=4) with Atomic Force Microscopy (AFM). Few AFM micrographs were selected to determine particles' size characteristics (see Fig. 6).

Biological polyanion	**D_{core} (nm)**	**D_{corona} (nm)**	**$D_{primary\ polyplexes}$ (nm)**
Calf-thymus DNA (CT-DNA)	108	114	18 ± 5
Heparin (HP)	67	114	13 ± 3
Chondroitin Sulfate (CS)	100	129	16 ± 3
Hyaluronic Acid (HA)	42	54	15 ± 4